HHS Public Access

Author manuscript

Cell Rep. Author manuscript; available in PMC 2024 July 30.

Published in final edited form as:

Cell Rep. 2024 July 23; 43(7): 114382. doi:10.1016/j.celrep.2024.114382.

Retrograde adenosine/A_{2A} receptor signaling facilitates excitatory synaptic transmission and seizures

Kaoutsar Nasrallah[1,6], **Coralie Berthoux**[1], **Yuki Hashimotodani**[1,4], **Andrés E. Chávez**[1,5], **Michelle Gulfo**[1], **Rafael Luján**[3], **Pablo E. Castillo**[1,2,*]

[1]Dominick P. Purpura Department of Neuroscience, Albert Einstein College of Medicine, Bronx, NY 10461, U.S.A.

[2]Department of Psychiatry & Behavioral Sciences, Albert Einstein College of Medicine, Bronx, NY 10461, U.S.A.

[3]Instituto de Investigación en Discapacidades Neurológicas (IDINE), Facultad de Medicina, Universidad Castilla-La Mancha, 02008 Albacete, Spain

[4]Present address: Graduate School of Brain Science, Doshisha University, Kyoto, Japan

[5]Present address: Centro Interdisciplinario de Neurociencia de Valparaíso, Facultad de Ciencias, Universidad de Valparaíso, Valparaíso 2340000, Chile

[6]Present address: Department of Biological Sciences, Fordham University, Bronx, NY 10458, U.S.A.

Summary

Retrograde signaling at the synapse is a fundamental way by which neurons communicate and neuronal circuit function is fine-tuned upon activity. While long-term changes in neurotransmitter release commonly rely on retrograde signaling, the mechanisms remain poorly understood. Here, we identified adenosine/A_{2A} receptor (A_{2A}R) as a retrograde signaling pathway underlying presynaptic long-term potentiation (LTP) at a hippocampal excitatory circuit critically involved in memory and epilepsy. Transient burst activity of a single dentate granule cell induced LTP of mossy cell synaptic inputs, a BDNF/TrkB-dependent form of plasticity that facilitates seizures. Postsynaptic TrkB activation released adenosine from granule cells, uncovering a non-conventional BDNF/TrkB signaling mechanism. Moreover, presynaptic A_{2A}Rs were necessary and sufficient for LTP. Lastly, seizure induction released adenosine in a TrkB-dependent manner, while removing A_{2A}Rs or TrkB from the dentate gyrus had anti-convulsant effects. By mediating

*To whom correspondence should be addressed (Lead Contact): Pablo E. Castillo, MD/PhD, Dominick P. Purpura Department of Neuroscience, Albert Einstein College of Medicine, 1410 Pelham Parkway South, Kennedy Center, Room 703, Bronx, NY 10461, USA, pablo.castillo@einsteinmed.edu.

Author contributions

K.N. and P.E.C. designed studies and wrote the manuscript. K.N. performed experiments and analyzed all data except for the *in vitro* adenosine measurements that were designed, performed, and analyzed by C.B.. R.L. performed and analyzed immunoelectron microscopy experiments. M.G. tested the role of A1 receptors. Y.H and A.C designed, performed, and analyzed early experiments assessing conventional retrograde signals. All authors read and edited the manuscript.

Declaration of interest

The authors declare no competing interest.

presynaptic LTP, adenosine/$A_{2A}R$ retrograde signaling may modulate dentate gyrus-dependent learning and promote epileptic activity.

Keywords

Mossy cell; hippocampus; dentate gyrus; retrograde signaling; epilepsy; presynaptic; BDNF; TrkB; PKA; LTP

INTRODUCTION

Retrograde signaling at the synapse is a well-established mechanism whereby a neuron can strengthen or weaken the synaptic inputs it receives[1,2]. Diverse messengers, including lipids, gases, peptides, and conventional neurotransmitters, can be released from the postsynaptic neuron upon activity and activate presynaptic receptors or other molecular targets, establishing a retrograde signaling system that powerfully increases or decreases neurotransmitter release. Retrograde signaling has been implicated in short-term synaptic plasticity[1], presynaptic long-term plasticity[3,4], and presynaptic homeostatic plasticity[5], all of which rely on changes in neurotransmitter release. Despite the significance of retrograde signaling in fine-tuning neuronal circuit function, important knowledge gaps remain regarding the identity and release mechanism of the retrograde messenger, as well as the presynaptic targets and downstream molecular cascades implicated in regulating neurotransmitter release.

The dentate gyrus (DG), the primary input area of the hippocampus, contains two main types of excitatory neurons: dentate granule cells (GCs) and hilar mossy cells (MCs). MCs and GCs form an associative circuit proposed to play a key role in DG-dependent cognitive functions[6,7] and epilepsy[8–13]. Repetitive stimulation of MC axons with physiologically relevant activity patterns triggers robust presynaptic long-term potentiation at MC-GC synapses (MC-GC LTP) but not at MC to interneurons synapses[14]. Recent evidence indicates that MC-GC LTP can be induced *in vivo* by enriched environment exposure[15] and experimental epileptic activity[13]. Uncontrolled strengthening of MC-GC transmission promotes seizures and likely contributes to the pro-epileptic role of MCs in early epilepsy stages[12,13]. Thus, it is crucial to determine the precise mechanism underlying MC-GC LTP. This presynaptic form of plasticity is mechanistically unique. Its induction is NMDA receptor-independent but requires postsynaptic BDNF/TrkB signaling upstream of presynaptic cAMP/PKA signaling[14], strongly suggesting the involvement of a retrograde signaling system whose identity is unknown.

The following criteria must be satisfied to establish retrograde signaling as a mechanism of presynaptic long-term plasticity. First, the retrograde messenger must be synthesized and released from the postsynaptic compartment. Second, interfering with the synthesis or release of this messenger should prevent plasticity. Third, the target for the retrograde messenger must be present in the presynaptic bouton. Fourth, interfering with the presynaptic target should also prevent plasticity. Lastly, activation of the presynaptic target by the retrograde messenger or some analogous molecule should mimic long-term plasticity –although, in some cases, this activation alone may be insufficient to induce plasticity.

In this study, we sought to determine the retrograde signal involved in presynaptic LTP at MC-GC synapses. To our surprise, we found that most conventional retrograde messengers were not implicated in this form of plasticity. Using selective pharmacology, immunoelectron microscopy, and a conditional knockout strategy, we discovered that activation of presynaptic G_s-coupled adenosine A_{2A} receptors (A_{2A}Rs) is necessary and sufficient to induce MC-GC LTP. In addition, TrkB activation mobilized adenosine from GCs, uncovering a TrkB-dependent signaling mechanism, whereas interfering with adenosine release from GCs abolished LTP. Furthermore, adenosine was released *in vivo* during acutely induced epileptic seizures in a TrkB-dependent manner, while removing A_{2A}Rs or TrkB from hippocampal excitatory neurons had anti-convulsant effects. Our findings not only establish adenosine/A_{2A}R as a retrograde signaling system that mediates presynaptic plasticity but also uncover a synapse-specific mechanism by which BDNF/TrkB and A_{2A}Rs may promote epileptic activity.

RESULTS

Theta-burst firing of a single GC induces presynaptic LTP at MC-GC synapse

To identify the retrograde signal mediating MC-GC LTP, we first tested whether activation of a single GC, a manipulation previously used to characterize endocannabinoid retrograde signaling in long-term plasticity[16], could trigger MC-GC LTP. We found that GC theta-burst firing (TBF: 10 bursts at 5 Hz of 5 AP at 50 Hz, repeated 4 times every 5s, Figure 1A) induced LTP selectively at MC-GC synapses but not at neighboring medial perforant path (MPP)-GC synapses (Figure 1B). In addition, the group II mGluR agonist DCG-IV (1 μM), which selectively abolishes GC-MC[17] but not MC-GC synaptic transmission[18], did not affect the magnitude of TBF-induced LTP (Figure S1A), indicating that this plasticity does not rely on GC recruitment of MC firing. We then tested whether TBF-LTP shared the same mechanistic features as synaptically-induced MC-GC LTP. Like synaptically-induced MC-GC LTP[14], TBF-LTP is likely expressed presynaptically, as indicated by a significant reduction in both paired-pulse ratio (PPR) and coefficient of variation (CV) (Figure 1C) (see Methods). Moreover, TBF-LTP was abolished in the presence of the selective TrkB antagonist ANA-12 (15 μM) (Figure S1B) and in postsynaptic (Figure 1D and Figure S1C) but not presynaptic *TrkB* conditional knockout (cKO) mice (Figure S1D) (see Methods). TBF-LTP was also abolished in postsynaptic *Bdnf* cKO mice (Figure S1E), in GCs patch-loaded with botulinum toxin-B (Botox, 0.5 μM; Figure S1F), which blocks BDNF release[19], and in GCs loaded with the calcium chelator BAPTA (20 mM), which blocks postsynaptic calcium rise during TBF (Figure S1G). We discarded the possibility that alterations in GC membrane properties or basal transmitter release could underlie the lack of LTP in postsynaptic *Bdnf* cKO (Nasrallah et al., 2022) and postsynaptic *TrkB* cKO (Figure S1H and S1I). The PKA inhibitors H89 (10 μM, 40- to 60-min pre-incubation and bath applied) (Figure S1J) and membrane-permeable $PKI_{14–22}$ myristoylated (1 μM, 40- to 60-min pre-incubation and bath applied) (Figure 1E) also abolished TBF-LTP, whereas loading the membrane-impermeable PKI_{6-22} (2.5 μM) in GCs did not affect this plasticity (Figure 1E). Normal TBF-LTP was induced in the presence of the NMDAR antagonist D-APV (50 μM) (Figure S1K). Remarkably, while postsynaptic *TrkB* or *Bdnf* deletion abolished GC TBF-induced LTP (Figure 1D,1F and Figure S1C, E), it had no impact on the chemical LTP

induced by transient activation of PKA with the adenylyl cyclase activator forskolin[13–15], supporting the notion that PKA acts downstream of BDNF/TrkB. To remove *TrkB* from GC selectively, we took advantage of a lentivirus encoding Cre under the control of the C1ql2 promoter, which achieves sparse labeling of GCs (Figure S1C)[20,21]. In all, these manipulations (summarized in Figure 1F) indicated that, like synaptically-induced MC-GC LTP, TBF-LTP requires postsynaptic BDNF/TrkB signaling and presynaptic PKA signaling and is NMDAR-independent (Figure 1G). Lastly, synaptically-induced MC-GC LTP and TBF-LTP occluded each other (Figure S2), indicating a common mechanism. Thus, GC TBF triggered a presynaptic form of LTP with identical properties to the synaptically induced MC-GC LTP[14], thereby establishing a simple, single-cell manipulation to investigate the identity of the retrograde messenger (Figure 1G).

A non-conventional retrograde signal likely mediates presynaptic LTP at MC-GC synapses

Previous work discarded endocannabinoids, glutamate, and GABA as retrograde signals mediating MC-GC LTP[14,22], and our current finding showing that normal TBF-LTP was induced in presynaptic *TrkB* cKO mice (Figure S1D) also discards BDNF as a retrograde messenger. We therefore tested the role of other conventional retrograde messengers, such as nitric oxide (NO) and lipid-derived messengers[1]. Application of the NO synthase inhibitor L-NAME (100 μM, 50- to 90-min pre-incubation and bath applied) did not impair TBF-LTP (Figure S3A), but significantly reduced LTP at CA3-CA1 synapses (Figure S3B), as previously reported[23]. Blockade of lipid-derived messengers with a cocktail of inhibitors consisting of the fatty acid amide hydrolase (FAAH) and anandamide amidase inhibitor AACOCF3 (10 μM, 50- to 80-min pre-incubation and bath applied), the lipoxygenases inhibitor baicalein (3 μM, 50- to 80-min pre-incubation and bath applied), and the lipase inhibitor THL (tetrahydrolipstatin or orlistat, 4 μM in the recording pipette) did not impair TBF-LTP either (Figure S3C). As positive controls, we found that both AACOCF3 and baicalein significantly reduced long-term depression (LTD) at CA3-CA1 synapses (Figure S3D)[24], and loading the lipase inhibitor THL (4 μM) in the recording pipette efficiently blocked CA1 inhibitory LTD (iLTD) (Figure S3E)[25]. Lastly, as was true for TBF-LTP, blocking NO signaling and lipid-derived messengers in interleaved control experiments did not alter synaptically-induced LTP either (Figure S4). Altogether, our results strongly suggest the involvement of a non-conventional retrograde messenger in presynaptic MC-GC LTP.

Presynaptic A_{2A}Rs are required for MC-GC LTP

Presynaptic PKA signaling is necessary and sufficient to induce LTP of MC-GC synaptic transmission[14], raising the possibility that the retrograde messenger induces LTP by activating a G_s-coupled G protein-coupled receptor (GPCR) located on MC axon terminals. The G_s-coupled adenosine A_{2A} receptor (A_{2A}R) is a good candidate as it has been implicated in BDNF-mediated plasticity at other synapses[26–28], and the endogenous ligand adenosine can be released from neurons upon activity[29–33]. To test whether adenosine mediates MC-GC LTP by activating presynaptic A_{2A}Rs, we first examined whether A_{2A}R antagonism impaired this plasticity. Two different A_{2A}R antagonists, SCH 58261 (100 nM) and ZM241385 (50 nM), abolished TBF-LTP (Figure 2A). Moreover, bath application of SCH 58261 did not change basal transmission (Figure 2B) but prevented the induction

of LTP by BDNF puffs (8 nM, 2 puffs of 3 s) delivered in the inner molecular layer (IML) (Figure 2C)[14], strongly suggesting that $A_{2A}R$ activation is required downstream of the BDNF/TrkB cascade. It is unlikely that postsynaptic $A_{2A}Rs$ could be implicated, given that including the GPCR inhibitor GDPβS (1 mM) in the recording pipette did not affect TBF-LTP. In contrast, as a positive control, it abolished the change in holding current induced by the selective GABAb receptor agonist baclofen (10 μM) (Figure 2D). Likewise, synaptically-induced MC-GC LTP was also abolished by SCH 58261 (Figure S5A) but not by including GDPβS in the recording pipette (Figure S5B). To demonstrate the role of presynaptic $A_{2A}Rs$ in MC-GC LTP, we also employed a conditional knockout strategy combined with optogenetics, which allowed us to selectively activate $A_{2A}R$-deficient MC axons expressing the fast opsin ChIEF (Figure 2E). We found that synaptic responses elicited by the activation of these axons did not undergo TBF-LTP (Figure 2F). In contrast, deleting *Adora2a* from MCs did not significantly affect basal neurotransmitter release, as indicated by the lack of PPR change (Figure 2G). Taken together, these findings indicate that presynaptic and not postsynaptic $A_{2A}R$ activation is necessary for LTP at MC-GC synapses.

Activation of presynaptic $A_{2A}Rs$ is sufficient to induce MC-GC LTP

Next, we tested whether $A_{2A}R$ activation was sufficient to induce LTP at MC-GC synapses. Bath application of the $A_{2A}R$ agonist CGS21680 (50 nM, 15 min) selectively enhanced MC but not MPP EPSC amplitude (Figure 3A). This synapse-specific potentiation was associated with a significant decrease in both PPR and CV (Figure 3B), suggesting a presynaptic mechanism of expression and supporting a presynaptic location of $A_{2A}Rs$. In addition, we tested whether supramammillary (SuM) inputs express functional $A_{2A}Rs$ using optogenetic activation of SuM inputs[34] (see Methods). Unlike MC EPSCs, SuM EPSCs were not enhanced by CGS21680 bath application (Figure 3C). We then directly assessed the contribution of presynaptic $A_{2A}Rs$ at MC-GC synapses by testing CGS21680-induced potentiation in presynaptic $A_{2A}Rs$ cKO mice. CGS21680 failed to increase MC-GC synaptic transmission in presynaptic *Adora2a* cKO mice (Figure 3D). Adding the selective $A_{2A}R$ antagonist SCH 58261 (100 nM) during the washout of CGS21680 (50 nM) did not impair the long-lasting potentiation, whereas continuous bath application of SCH 58261 (100 nM) abolished the CGS21680-induced potentiation (Figure 3E). These results indicate that activation of presynaptic $A_{2A}Rs$ was sufficient to induce LTP at MC-GC synapses.

Because the $A_{2A}R$ is a G_s-coupled receptor, we next tested whether CGS21680-induced LTP was PKA-dependent. Bath application of the selective, cell-permeable PKA inhibitor myristoylated $PKI_{14\text{-}22}$ (1 μM)[35] abolished CGS21680-induced LTP, whereas loading the membrane-impermeable PKA inhibitor $PKI_{6\text{-}22}$ (2.5 μM) in GCs via the recording pipette[14,36] had no effect (Figure 3F), suggesting that presynaptic but not postsynaptic PKA activity is required for the $A_{2A}R$ agonist-mediated strengthening of MC-GC synaptic transmission. While deleting $A_{2A}Rs$ from MCs blocked both GC TBF-LTP (Figures 2E and 2F) and CGS21680-LTP (Figure 3D), we found that forskolin induced normal LTP in presynaptic *Adora2a* cKO mice (Figure 3G). Altogether, these findings indicate that presynaptic $A_{2A}R$ activation enhances glutamate release via presynaptic PKA activation, consistent with previous results showing that PKA activity is necessary and sufficient for MC-GC LTP (Figure 1E–1G, Figure S1J)[14].

Our results thus far indicate that both BDNF/TrkB and adenosine/A_{2A}R signaling are involved in MC-GC LTP, and previous work demonstrated that A_{2A}Rs facilitate BDNF signaling at some synapses[26]. We, therefore, sought to determine potential interactions between these signaling cascades at the MC-GC synapse. The TrkB antagonist ANA-12 did not affect CGS21680-induced LTP (Figure 3H), whereas it blocked TBF-LTP in interleaved experiments (Figure 3I; see also Figure S1B). Lastly, we found that pre-application of CGS21680 (50 nM, 15 min) occluded both BDNF puff-induced and GC TBF-induced LTP (Figure 3J and 3K), strongly suggesting that A_{2A}R agonism, BDNF, and GC TBF strengthen MC-GC synapses via a common mechanism. These findings, together with our previous results (Figure 2), indicate that presynaptic adenosine/A_{2A}R signaling mediates LTP downstream of BDNF/TrkB signaling (Figure 3L).

Activation of presynaptic A_1Rs dampens MC-GC LTP

So far, our data indicate that the release of endogenous adenosine induces MC-GC LTP by activating presynaptic A_{2A}Rs (Figures 2 and 3). In addition to activating presynaptic A_{2A}Rs, adenosine could also activate presynaptic type 1 adenosine receptors (A_1Rs), $G_{i/o}$-coupled receptors known to suppress neurotransmitter release. To test the role of A_1Rs in MC-GC plasticity, we first used the selective A_1R antagonist DPCPX (100 nM). DPCPX increased MC-GC LTP magnitude (Figure S6A) but did not affect basal transmission (Figure S6B), indicating that adenosine acts on A_1Rs to dampen MC-GC LTP induction, but A_1Rs are not tonically activated by adenosine. In addition, we considered that A_1Rs could mediate presynaptic LTD[37]. However, bath application of the selective A_1R agonist CCPA (50 nM, 15 min) reduced both MC and MPP-mediated transmission reversibly as the reduction was washed out with the A_1R antagonist DPCPX (100 nM) (Figure S6C). This transient A_1R-induced depression was associated with a reversible increase in both PPR and CV (Figures S6D and S6E), suggesting a presynaptic mechanism. Of note, A_{2A}R antagonism blocked TBF-LTP induction, but MC-GC transmission was not reduced in a long-term manner (Figure 2A), indicating that the net effect of adenosine released during GC TBF is to potentiate MC-GC transmission through A_{2A}R activation. Individual MC boutons could contain both A_1 and A_{2A} receptors. To test this possibility, we examined whether responses elicited by minimal stimulation, a manipulation known to activate one to three MC-GC synapses impinging on GCs[14], were sensitive to both A_{2A}R and A_1R agonists. We found that the A_{2A}R agonist CGS21680 (50 nM) potentiated the synaptic responses evoked by minimal stimulation of MC axons, whereas subsequent application of the A_1R agonist CCPA (50 nM) significantly reduced these potentiated responses recorded from the same GC (Figure S6F and S6G). These results strongly suggest that functional A_1 and A_{2A} receptors colocalize in the same MC axon boutons.

Anatomical evidence for A_{2A} and A_1 receptors in MC axon terminals

To test whether MC terminals express A_1 and A_{2A} receptors, we performed immunoelectron microscopy. Immunoparticles for A_1Rs were mainly found presynaptically in the molecular layer of the dentate gyrus at MC-GC and perforant path (PP)-GC synapses (Figures 4A, 4B, 4C and 4D). Remarkably, using an anti-A_{2A}R antibody previously validated in A_{2A}R-deficient mice[38], we found strong A_{2A}R expression in the presynaptic membrane of asymmetric (presumably glutamatergic) synapses and very few postsynaptic particles in

the IML (Figures 4E, 4F and 4H). In contrast, a quasi-exclusive postsynaptic expression was detected at asymmetric PP-GC synapses (Figures 4G, 4I and 4H). Given the strong projection of MC axons in the IML[39], the presynaptic $A_{2A}R$ labeling most likely arises from MC axon boutons. While the antibodies were not validated in the DG using immunoelectron microscopy, these anatomical results are consistent with our functional findings. Although both A_1 and A_{2A} receptors are expressed at MC axon terminals, only the latter engages long-lasting synaptic plasticity.

Passive adenosine release from GC is required for presynaptic MC-GC LTP

We next sought to determine the source of adenosine that triggers $A_{2A}R$-mediated LTP. Adenosine can be released from neurons upon activity[29,31–33] via equilibrative nucleoside transporters (ENTs)[30]. If adenosine is the retrograde signal mediating MC-GC LTP, interfering with adenosine release from GCs by blocking ENTs should impair LTP. As a first approach, we tested whether blocking ENTs can interfere with LTP induction. Bath application of the ENT inhibitors dipyridamole (20 μM) and NBMPR (10 μM) abolished LTP (Figure 5A) but did not affect basal MC-GC synaptic transmission (Figure 5B). Because ENTs are also implicated in adenosine reuptake, bath application of the ENT blockers may significantly increase extracellular adenosine levels, which, by activating $A_{2A}Rs$, may potentiate MC-GC transmission and occlude LTP. Further, the fact that ENT blockers did not affect basal MC-GC synaptic transmission (Figure 5B) could be due to the simultaneous activation of A_1R, which might mask any potential $A_{2A}R$-mediated potentiation. To test this possibility, we bath applied both the ENT blockers and DPCPX (100 nM) to prevent a potential A_1R-mediated depression of MC-GC synaptic transmission. We found that co-application of the ENT blockers and DPCPX (100 nM) increased MC-GC transmission, and this effect was abolished in the presence of the $A_{2A}R$ antagonist SCH 58261 (100 nM) (Figure 5C). These results indicate that endogenous adenosine can activate presynaptic $A_{2A}Rs$ to potentiate MC-GC synaptic transmission.

To directly test whether postsynaptic adenosine release is required for MC-GC LTP, we employed a single-cell approach and selectively blocked ENTs in a single GC. Like previous studies[31,33], we loaded inosine (100 μM), a competitive blocker of adenosine efflux through ENTs[30], intracellularly *via* the recording pipette. We found that intracellular inosine abolished TBF-LTP (Figure 5D), whereas bath application of 100 μM inosine did not affect MC-GC synaptic transmission (Figure 5E). Bath application of DPCPX increased MC EPSC amplitude when ENT inhibitors were continuously bath applied but not when inosine (100 μM) was loaded in a single GC (Figure 5F), confirming that intracellular inosine did not increase adenosine tone. Intracellular accumulation of adenosine can result from sequential dephosphorylation of ATP[40]. Consistent with this possibility, removing ATP from the internal recording solution abolished LTP (Figure 5G). Altogether, these findings indicate that adenosine, passively released from GC through ENTs, acts as a retrograde messenger at MC-GC synapses (Figure 5H).

Repetitive neuronal activity induces adenosine release via a BDNF/TrkB-dependent mechanism

To visualize adenosine release during MC-GC LTP induction, we utilized the genetically encoded sensor for adenosine $GRAB_{Ado1.0m}$[41,42], which was selectively expressed in commissural MC axons (see Methods) and generated a clear fluorescence signal in the contralateral IML (Figures 6A, 6B and 6D). The MC burst stimulation protocol that triggers synaptically-induced MC-GC LTP in acute hippocampal slices also triggered a robust, albeit transient, increase in the $GRAB_{Ado1.0m}$ signal. As expected[41], this enhancement was abolished when the MC BS protocol was delivered in the presence of the $A_{2A}R$ antagonist SCH58261 (Figures 6B, 6C and 6F). Consistent with $A_{2A}R$ signaling being engaged downstream of TrkB activation, the burst-induced increase of the $GRAB_{Ado1.0m}$-mediated fluorescence was abolished in the presence of the TrkB antagonist ANA-12 (15 μM), and in postsynaptic *TrkB* cKO and *Bdnf* cKO mice (Figures 6D–6F). These results demonstrate that MC repetitive activity releases adenosine in a BDNF/TrkB-dependent manner.

In vivo activation of A_{2A}Rs facilitates seizure occurrence

We recently found that MC-GC LTP can be triggered by seizure activity induced with kainic acid (KA) intraperitoneal (i.p.) administration and that this LTP further promotes seizures[13]. Given our new findings that neuronal activity releases adenosine via TrkB to induce $A_{2A}R$-dependent MC-GC LTP, we hypothesized that interfering with adenosine/$A_{2A}R$ signaling should prevent seizure-induced LTP and reduce KA-induced seizures. Moreover, seizure activity should release adenosine in a TrkB-dependent manner. As expected for a presynaptic form of plasticity, seizure-induced LTP increases neurotransmitter release, as indicated by a decrease in PPR[13]. While *Adora2a* deletion from MC axons did not alter basal PPR (Figure 2G), it prevented the KA-induced decrease in PPR (Figures 7A and 7B). These results indicate that presynaptic $A_{2A}Rs$ mediate seizure-induced LTP at MC-GC synapses. Moreover, *Adora2a* deletion increased latency to KA-induced convulsive seizures (Figures 7C–7F), and *TrkB* deletion increased latency to convulsive seizures and reduced sum seizure score (Figures 7G and 7H). These results strongly suggest that both $A_{2A}Rs$ and TrkB are proconvulsant, consistent with the seizure-induced release of adenosine in a TrkB-dependent manner.

Using *in vivo* two-photon imaging in awake mice, we recently reported that KA-induced seizures robustly increase MC and GC activity[13]. To test whether seizure activity triggers a TrkB-dependent release of adenosine *in vivo*, we expressed $GRAB_{Ado1.0m}$ in commissural MC axons and recorded the fluorescence signals using fiber photometry in freely moving mice (Figures 7I and 7J). We found a large increase in $GRAB_{Ado1.0m}$ fluorescence following i.p. injection of KA, and this fluorescence signal was significantly reduced in *TrkB* cKO mice (Figures 7K and 7L). Of note, both control and *TrkB* cKO mice reached stage 3 convulsive seizures, discarding potential failure of seizure induction. Altogether, these results demonstrate the TrkB-mediated in vivo release of adenosine following initial seizures and strongly suggest that adenosine signaling may promote seizures via $A_{2A}Rs$.

DISCUSSION

In this study, we discovered a retrograde signaling mechanism that mediates presynaptic strengthening within a critical hippocampal circuit (Figure S7). Specifically, repetitive firing of a single postsynaptic neuron was sufficient to trigger presynaptic LTP at MC-GC but not neighboring MPP synapses. We demonstrated that functional A_{2A}Rs are expressed at MC axon terminals but not at MPP axon terminals and that A_{2A}R activation is necessary and sufficient to induce MC-GC LTP. During LTP induction, GCs passively release adenosine through ENTs in a postsynaptic TrkB- and activity-dependent manner. Thus, our findings establish adenosine/A_{2A}R as a retrograde signaling mechanism. Remarkably, our results uncovered that TrkB can signal through adenosine. Moreover, we found that adenosine is released *in vivo* during initial seizures in a TrkB-dependent manner, and both *Adora2a* and *Trkb* cKOs have anti-convulsant effects.

GC TBF induces presynaptic LTP at MC-GC synapses

The present study revealed that direct activation of a single GC with a physiologically relevant pattern of activity[43–48] was sufficient to induce presynaptic LTP at MC-GC synapses without changing the strength of MPP neighboring inputs. Although the activity of a single GC could have induced LTP by recruiting the recurrent GC-MC-GC circuit, the following two observations are against this possibility. First, GC TBF induced normal LTP even in the continuous presence of the selective group II mGluR agonist DCG IV, which abolishes GC-MC[17] but not MC-GC transmission[18]. Second, TBF-LTP was normally induced at optogenetically-activated synaptic inputs arising from contralateral MC axons cut off from their cell bodies in hippocampal slices. TBF-LTP and synaptically-induced LTP likely share a common mechanism (Figure S2). Like synaptically-induced MC-GC LTP, which requires BDNF release from GCs[15], we now report that TBF-LTP requires postsynaptic calcium rise and BDNF release via SNARE-dependent exocytosis[19,49]. While synaptically-induced LTP is an input-specific phenomenon[14], TBF-induced LTP is not, likely reflecting the dissimilar induction protocols. Presynaptic burst stimulation releases adenosine from the postsynaptic compartment of activated synapses only. In contrast, TBF is expected to release adenosine from multiple synapses due to action potential-driven release of BDNF from GCs and autocrine activation of postsynaptic TrkB[15].

Adenosine is released from GCs in an activity and TrkB-dependent manner

Using the genetically encoded adenosine sensor $GRAB_{Ado1.0m}$[41,42], we detected a phasic increase in extracellular adenosine following both MC-GC LTP induction *ex vivo* and during seizure activity *in vivo*. Importantly, adenosine release required intact BDNF/TrkB signaling (Figure 6D–6F, Figure 7K and 7L). Previous studies have shown that adenosine can be released from neurons upon activity via ENTs[29–33,42]. In support of this mechanism, we found that interfering with the ENT-mediated release of adenosine from a single postsynaptic GC, or excluding ATP from the internal recording solution, abolished MC-GC LTP, indicating that the passive release of adenosine from GCs is essential for this form of plasticity. Adenosine arising from ATP extracellular conversion[50,51] or other cell types, such as interneurons and glial cells[29,52], could also strengthen MC-GC synaptic transmission.

Intracellular adenosine accumulation can result from sequential dephosphorylation of ATP or the hydrolysis of S-adenosylho-mocysteine[40]. During MC-GC LTP induction, the formation of intracellular adenosine in GCs likely results from robust postsynaptic TrkB activation and sequential dephosphorylation of ATP through its kinase activity. The following observations support this scenario. First, postsynaptic ATP is required for MC-GC LTP (Figure 5F). Second, MC-GC LTP induction releases BDNF that activates postsynaptic TrkB on GCs[14,15]. Third, activity-induced adenosine release in the IML is postsynaptic BDNF/TrkB-dependent, as it is abolished in the presence of the TrkB selective antagonist ANA-12 and by genetically removing *Bdnf* and *TrkB* from GCs (Figure 6D–6F and Figure 7I–L). Fourth, adenosine/A_{2A}R signaling is engaged downstream of TrkB activation, given that BDNF-induced LTP was abolished by A_{2A}R antagonism (Figure 2C), whereas TrkB antagonism did not affect A_{2A}R agonist-induced LTP (Figure 3E). Lastly, while BDNF activates postsynaptic TrkB[14,15] and adenosine acts via presynaptic A_{2A}Rs to induce MC-GC LTP, we cannot discard physical interaction or transactivation, a process whereby A_{2A}R activation can induce TrkB phosphorylation in the absence of neurotrophins[53].

To our knowledge, we provided the first direct evidence that adenosine release can occur in a TrkB-dependent manner. Such a mechanism could explain, at least in part, BDNF and adenosine signaling interactions reported at other synapses in the brain. Previous studies in the CA1 area have shown that A_{2A}Rs can affect synaptic transmission and plasticity by modulating BDNF-TrkB signaling[27,28,54]. Such modulation has recently been implicated in adult neurogenesis[55]. While these studies suggest that A_{2A}Rs act upstream of BDNF, our findings demonstrate that BDNF/TrkB signaling can also act upstream of A_{2A}Rs by promoting adenosine release. Consistent with our findings at the hippocampal MC-GC synapse, BDNF-induced facilitation at the neuromuscular junction was abolished in the presence of A_{2A}R antagonists but also by PKA inhibitors, while A_{2A}R agonist-induced increase in neurotransmitter release is TrkB-independent[26,56,57]. In conclusion, our findings support a model whereby neuronal activity releases adenosine in a TrkB-dependent manner, and therefore, adenosine release emerges as a non-canonical TrkB signaling mechanism. Further work is required to determine the generalizability of this model in other brain areas.

Retrograde adenosine/A_{2A}R signaling mediates presynaptic LTP

Retrograde signaling is a common mechanism in presynaptic forms of long-term plasticity[3,4]. While several retrograde signals have been identified throughout the brain[1], we uncovered adenosine/A_{2A}R as a form of retrograde signaling. Single-cell manipulations revealed that interfering with adenosine release from a single postsynaptic neuron abolished MC-GC LTP induced by GC firing alone. Furthermore, by combining pharmacology, presynaptic *Adora2a* deletion using cKO mice, and immunoelectron microscopy, we demonstrated that activation of presynaptic A_{2A}Rs was necessary and sufficient for MC-GC LTP. Despite the relatively low expression levels of A_{2A}R in the hippocampus[58], previous work has shown that A_{2A}R signaling can regulate hippocampal synaptic plasticity[59,60]. To our knowledge, our study provides the first evidence of adenosine/A2AR as a retrograde signaling system and that this signaling system can mediate presynaptic LTP. As G_s-coupled receptors, and as supported by our findings, A_{2A}Rs on MC axon terminals likely activate the cAMP/PKA cascade, and as for other forms of presynaptic LTP[3], this activation engages

a long-lasting increase of glutamate release whose downstream mechanism is poorly understood. Whether retrograde adenosine/A_{2A}R signaling can mediate activity-dependent strengthening at other synapses in the brain, including in the striatum and globus pallidus, where presynaptic A_{2A}Rs are highly expressed[61], remains to be investigated.

Retrograde adenosine/A_1Rs signaling dampens LTP induction

As previously reported at other synapses[56,62], our findings indicate that postsynaptically released adenosine simultaneously activates A_1Rs and A_{2A}Rs localized at MC terminals. A_1Rs and A_{2A}Rs can localize at the same nerve terminal[63] and even form heteromers[64]. While A_1R agonism transiently inhibited glutamate release, A_{2A}R agonism increased glutamate release in a long-lasting manner. Consistent with these pharmacological observations, the net effect mediated by the transient release of endogenous adenosine during LTP induction was a long-lasting enhancement of glutamate release. We also found A_1R-mediated dampening of LTP, which had previously been observed at other synapses[65,66]. A possible explanation for this dampening is that presynaptic A_1Rs, which are $G_{i/o}$-coupled, decrease the level of cAMP required for MC-GC LTP[14]. Type 1 cannabinoid receptor, another $G_{i/o}$-coupled receptor highly expressed at MC axon terminals, also dampens MC-GC LTP[22]. Thus, the induction of this form of plasticity is tightly controlled by two distinct retrograde signals, adenosine and endocannabinoids, which dampen LTP induction by activating presynaptic Gi/o-coupled receptors. Both retrograde signals may prevent runaway activity of the MC-GC-MC recurrent excitatory circuit.

Adenosine/A_{2A}R retrograde signaling in the dentate gyrus has physiological and pathological relevance

Growing evidence indicates that MCs are critically involved in hippocampal-dependent learning[7]. For example, silencing MCs selectively impairs spatial memory retrieval[11] and novelty-induced contextual memory acquisition[67]. MC-GC LTP is a robust form of presynaptic plasticity that can be elicited *in vivo* upon experience[15] and may contribute significantly to learning and memory by changing information flow in the DG[14]. While GCs exhibit extremely sparse and selective firing in a single place field[45], we found that MC-GC LTP can be triggered by GC firing alone, suggesting that this plasticity could be implicated in the experience-driven refinement of DG circuitry and memory. Previous work indicates that adenosine/A_{2A}R signaling may contribute to hippocampal-dependent memory[60,64]. Our findings showing a pivotal role for adenosine/A_{2A}R signaling in MC-GC LTP could explain, at least in part, memory impairments found in both A_{2A}R antagonist-injected animals[68] and hippocampal *Adora2a* cKO animals[69]. Demonstrating the precise role of adenosine/A_{2A}R retrograde signaling at MC-GC synapses in memory requires selective manipulation of A_{2A}Rs at MC axon terminals using tools that are not currently available.

Adenosinergic signaling is critically involved in epilepsy[70]. Global A_{2A}R genetic deletion and selective A_{2A}R antagonism attenuate both the seizure progression[71,72] and seizure-induced neuronal damage[73–75]. In contrast, A_{2A}R activation lowers the seizure threshold[76], and increased A_{2A}R function promotes epilepsy[77]. Although the precise mechanism by which A_{2A}Rs participate in temporal lobe epilepsy remains unclear, our current findings provide a potential explanation for the pro-epileptic role of A_{2A}Rs, consistent with our

previous findings that initial seizures trigger MC-GC LTP and that uncontrolled LTP is sufficient to promote subsequent seizures[13]. The BDNF/TrkB-mediated release of adenosine from GCs and the consequent strengthening of MC-GC synaptic transmission may also explain, at least in part, the pro-epileptic role of BDNF/TrkB signaling[78]. Our current study demonstrating adenosine/A_{2A}R-dependent strengthening of MC-GC synapses reveals a mechanism whereby MC activity *may* contribute to early stages of temporal lobe epilepsy.

Limitations of the Study

The present study established adenosine/A_{2A}R as retrograde signaling mediating presynaptic long-term plasticity, such as MC-GC LTP. However, activation of postsynaptic A_{2A}Rs at PP-GC synapses and putative A_{2A}Rs in inhibitory interneurons could also modulate GC activity and DG function. The adenosine source and conditions that activate these receptors are unknown. We also found that presynaptic A_{2A}R mediated MC-GC synaptic strengthening during initial KA-induced seizures and that A_{2A}R removal from DG excitatory neurons was pro-convulsant. However, demonstrating the precise contribution of adenosine/A_{2A}R retrograde signaling at MC-GC synapses in triggering seizure activity requires synapse-specific molecular tools that are not currently available –e.g., selective removal of A_{2A}Rs from MC axon boutons. Such tools will also be critical to uncover how adenosine/A_{2A}R retrograde signaling can shape DG function. While we showed that adenosine was released from GCs in a postsynaptic TrkB and activity-dependent manner, how exactly TrkB activation generates adenosine in GCs remains to be determined. The $GRAB_{Ado}$ sensor revealed that adenosine was released during MC bursts and seizures. However, this sensor alone did not allow us to determine the adenosine source. This study did not address whether TrkB-dependent release of adenosine can occur in other cell types, including astrocytes. Lastly, the retrograde signaling described here may operate in different brain areas where presynaptic A_{2A}Rs are highly expressed, a possibility that remains to be tested.

STAR Methods

Resource Availability

Lead Contact—Further information and requests for resources and reagents should be directed to and will be fulfilled by the Lead Contact, Pablo E. Castillo (pablo.castillo@einsteinmed.edu).

Materials Availability—This study did not generate new unique reagents.

Data and Code Availability—All data reported in this paper will be shared by the lead contact upon reasonable request.

- This paper does not report any original code.

- Any additional information required to reanalyze the data reported in this work paper is available from the Lead Contact upon request.

Experimental Model and Study Participant Details

P19-P30 Sprague-Dawley rats and P50-P70 C57BL/6, floxed TrkB (*TrkB*$^{fl/fl}$), floxed BDNF (*Bdnf*$^{fl/fl}$), floxed *Adora2a* (*Adora2a*$^{fl/fl}$), and VGluT2-Cre mice (Jackson labs, Slc17a6$^{tm2(cre)Lowl}$/J, stock #016963) mice were used. Males and females were equally used. All animals were group housed in a standard 12 hr light/12 hr dark cycle and had free access to food and water. Animal handling and use followed a protocol approved by the Institutional Animal Care and Use Committee of Albert Einstein College of Medicine in accordance with the National Institutes of Health guidelines. Animal care and handling for immunoelectron microscopy studies followed a protocol approved by the Institutional Animal Care and Use Committee of Universidad Castilla-La Mancha in accordance with Spanish (RD 1201/2005) and European Union (86/609/EC) regulations. The supramammillary experiments were approved by the Animal Care and Use Committee of Doshisha University and were performed following the committee guidelines. *TrkB*$^{fl/fl}$ and *Bdnf*$^{fl/fl}$ mice generated by Dr. Luis Parada were kindly donated by Dr. Lisa Monteggia (University of Texas, Southwestern Medical Center). *Adora2*$^{fl/fl}$ were obtained from Jackson Laboratory (B6;129-Adora2atm1Dyj/J, Jax 010687).

Method Details

Hippocampal slice preparation—Acute transverse hippocampal slices were prepared from Sprague-Dawley rats (400 μm thick) and mice (300-μm thick). Animals were anesthetized with isofluorane and euthanized following institutional regulations. The hippocampi were then removed and cut using a VT1200s microslicer (Leica Microsystems Co.) in a cutting solution. Hippocampal slices from rats were prepared using a cutting solution containing (in mM): 215 sucrose, 2.5 KCl, 26 $NaHCO_3$, 1.6 NaH_2PO_4, 1 $CaCl_2$, 4 $MgCl_2$, 4 $MgSO_4$ and 20 D-glucose. 30 min post-sectioning, the cutting medium was gradually switched to an extracellular artificial cerebrospinal (ACSF) recording solution containing (in mM): 124 NaCl, 2.5 KCl, 26 $NaHCO_3$, 1 NaH_2PO_4, 2.5 $CaCl_2$, 1.3 $MgSO_4$ and 10 D-glucose. Slices were incubated for at least 40 min in the ACSF solution before recording. Mouse hippocampal slices were prepared using an NMDG-based cutting solution containing (in mM): 93 N-Methyl-d-glucamin, 2.5 KCl, 1.25 NaH_2PO_4, 30 $NaHCO_3$, 20 HEPES, 25 D-glucose, 2 Thiourea, 5 Na-Ascorbate, 3 Na-Pyruvate, 0.5 $CaCl_2$, 10 $MgCl_2$. These slices were then transferred to 32°C ACSF for 30 min and then kept at room temperature for at least 1h before recording. All solutions were equilibrated with 95% O_2 and 5% CO_2 (pH 7.4).

Electrophysiology—Recordings were performed at 28 ± 1 °C, otherwise stated, in a submersion-type recording chamber perfused at 2 mL/min with ACSF supplemented with the $GABA_A$ and the $GABA_B$ receptor antagonists, picrotoxin (100 μm) and CGP55845 hydrochloride (3 μm), respectively. Whole-cell patch-clamp recordings using a Multiclamp 700A amplifier (Molecular Devices) were obtained from GCs voltage clamped at −60 mV using patch-type pipette electrodes (~3-4 MΩ) containing a potassium-based internal solution (in mM): 135 $KMeSO_4$, 5 KCl, 1 $CaCl_2$, 5 NaOH, 10 HEPES, 5 MgATP, 0.4 Na_3GTP, 5 EGTA and 10 D-glucose, pH 7.2 (288-291 mOsm). For IPSC recordings in CA1, whole-cell voltage clamp recordings were obtained from CA1 pyramidal neurons voltage clamped at V_h= 10 mV using a cesium-based internal solution containing (in mM):

131 cesium gluconate, 8 NaCl, 1 $CaCl_2$, 10 EGTA, 10 D-glucose and 10 HEPES, pH 7.2 (285-290 mOsm). IPSCs were evoked using an electrical stimulating pipette placed in the CA1 *stratum radiatum*, and recordings were performed in the continuous presence of ionotropic glutamate receptor antagonists NBQX (10 μM) and D-APV (50 μM). LTD of inhibitory inputs onto CA1 pyramidal neurons (iLTD) was induced using theta burst-stimulation protocol (TBS, 10 bursts at 5 Hz of 5 pulses at 100 Hz, repeated every 5 s, 4 times). Series resistance (~6-25 MΩ) was monitored throughout all experiments with a −5 mV, 80 ms voltage step, and cells that exhibited a significant change in series resistance (> 15%) were excluded from the analysis. Botox experiments were performed at 32°C. Botox was supplemented with 5 mM dithiothreitol (DTT) in the intracellular solution, and interleaved control experiments included DTT only.

A broken tip (~10–20 μm) stimulating patch-type micropipette filled with ACSF was placed in the inner molecular layer (IML, < 50 μm from the border of the GC body layer) to activate MC axons, and in the middle third of the molecular layer to activate MPP inputs. For minimal stimulation (Figure S6F and S6G), stimulating pipettes were made from theta glass capillaries. To elicit synaptic responses, paired, monopolar square-wave voltage or current pulses (100–200 μs pulse width, 4-27 V) were delivered through a stimulus isolator (Digitimer DS2A-MKII). Typically, stimulation intensity was adjusted to obtain synaptic responses comparable in amplitude across experiments, e.g., 30-70 pA EPSCs (V_h −60 mV). For the optogenetic experiments, EPSCs were evoked using 1-3 ms pulses of blue (470-nm) light, provided by a collimated LED (Thorlabs, M470L3-C5, 470 nm, 300mW) and delivered through the microscope objective (40X, 0.8 NA). GC TBF-induced LTP was typically induced with 10 bursts at 5 Hz of 5 AP at 50 Hz, repeated 4 times every 5s, while the membrane potential was held at −60 mV in current-clamp mode. Extracellular field excitatory postsynaptic potentials (fEPSPs) were recorded using patch-type pipettes filled with 1M NaCl, and placed in *CA1 stratum radiatum*. fEPSPs were evoked with an ACSF-containing broken tip patch pipette in the *CA1 stratum radiatum*. LTP at CA3-CA1 synapses was triggered using high frequency stimulation protocol (4 HFS: 100 pulses at 100 Hz repeated 4 times every 10 s) and recordings were performed at 25 ± 1°C. LTD was induced with a low-frequency stimulation protocol (LFS: 900 pulses at 1 Hz).

Electrophysiological data were acquired at 5 kHz, filtered at 2.4 kHz, and analyzed using custom-made software for IgorPro (Wavemetrics Inc.). Paired-pulse ratio (PPR) was defined as the ratio of the amplitude of the second EPSC (baseline taken 1-2 ms before the stimulus artifact) to the amplitude of the first EPSC. The coefficient of variation (CV) was calculated as the standard deviation of EPSC amplitude divided by the mean EPSC amplitude. Both PPR and CV were measured 10 min before and 20–30 min after LTP induction protocol or CGS21680-induced potentiation. PPR and CV were measured over minutes 0-6 before, 9-15 min after, and 29-35 min after CCPA application. The magnitude of LTP/LTD was determined by comparing 10 min baseline responses with responses 20-30 min (or 30-40 min for Figure 1B, 40-50 min for Figure 2B, 45-55 min for Figure 2D) after induction protocol. Averaged traces include 20 consecutive individual responses.

Postsynaptic *TrkB* and *Bdnf* conditional KO—Adeno-associated virus AAV_5.CamKII.eGFP (control virus) or AAV_5.CamKII.GFP-CRE (University of

Pennsylvania Vector Core) was injected (1 μL at a flow rate of 0.1 μL/min) unilaterally into the dorsal blade of the dentate gyrus (2.06 mm posterior to bregma, 1.5 mm lateral to bregma, 1.8 mm ventral from dura) of *TrkB*$^{fl/fl}$ or *Bdnf*$^{fl/fl}$ mice (4-5 week old). Animals were placed in a stereotaxic frame and anesthetized with isoflurane (up to 5% for induction and 1%–3% for maintenance). Slices for electrophysiology were prepared from injected animals 3–5 weeks after injection. The absence of GFP-expressing cells in the hilus of the entire ipsilateral hippocampus was verified for each animal. We previously reported that this strategy can target GCs almost exclusively, as indicated by the lack of labeling in the hilus[13–15]. To conditionally KO *TrkB* from GCs, we also injected a control (ChiEFtom2A-GFP) or a Cre-expressing lentivirus selective for GCs (ChIEFtom2A-Cre, Post TrkB cKO) into the DG (relative to bregma: 1.9 mm posterior, 1.25 mm lateral, 2.3 ventral) of *TrkB*$^{fl/fl}$ mice (see Figure S1C). The lentivirus encoding ChiEFtom2A-Cre or ChiEFtom2A-GFP was under the control of the GC-specific C1ql2 promoter[20], which was successfully used in our lab[21]. In all cases, MC EPSCs were monitored in glowing GCs. C1ql2-ChiEFtom2A-GFP or C1ql2-ChiEFtom2A-Cre plasmids were a gift of Drs. Gaël Barthet and Christophe Mulle, Université de Bordeaux, and lentiviruses were made at the Einstein Genetic Engineering and Gene Therapy Core.

Presynaptic *TrkB* and *Adora2a* conditional KO—A mix (1:2 ratio, 1.2 μL at 0.1 μL/min) of Cre recombinase-containing AAV (AAV5.CaMKII.Cre-mCherry, UNC Vector) and Cre-dependent ChiEF (AAV_{DJ}.Flx.ChIEF.TdTomato) was injected into the dentate gyrus (relative to bregma: 1.9 mm posterior, 1.25 mm lateral, 2.3 ventral) of adult *TrkB*$^{fl/fl}$, *Adora2a*$^{fl/fl}$ or WT control mice (4-5 week old). We then performed electrophysiology experiments 4-5 weeks post-injection in contralateral hippocampal slices. This allowed us to optically activate Cre-expressing MC axons.

Optogenetic activation of supramammillary inputs—A beveled glass capillary pipette connected to a microsyringe pump (UMP3, WPI) was used for viral injection. 200 nL (50 nL/min) of AAV1-EF1a-DIO-hChR2(H134R)-eYFP (Addgene: 20298-AAV1) was injected into the SuM (relative to bregma, AP: −2.2 mm, ML: ±0.3 mm, DV: −4.85 mm) of VGluT2-Cre mice. The glass capillary remained at the target site for 5 min before the beginning of the injection and was removed 10 min after the infusion. Channelrhodopsin (ChR2)-expressing SuM axons were activated at 0.05 Hz by a pulse of 470 nm blue light (5 ms duration, 10.5 mW/mm^2) delivered through a 40X objective attached to a microscope using an LED (Mightex).

Pharmacology—Reagents were bath-applied following dilution into ACSF from stock solutions stored at −20°C prepared in water, DMSO or ethanol, depending on the manufacturer's recommendation. BDNF puffs (8 nM, 2.5-3 PSI, 3 s puffs repeated twice, 5 s interval) were applied using a Picospritzer III (Parker) connected to a broken patch pipette. The tip of the puffer pipette was positioned above the IML while monitoring MC-GC transmission. For experiments requiring postsynaptic loading PKI_{6-22}, LTP was induced at least 20 min after establishing the whole-cell configuration. The time to the LTP induction was matched in interleaved controls.

Electron Microscopy—Mice were anesthetized by intraperitoneal injection of ketamine/xylazine (ratio 1:1, 0.1 mL/kg) and transcardially perfused with an ice-cold fixative containing 4% paraformaldehyde, with 0.05% glutaraldehyde and 15% (v/v) saturated picric acid made up in 0.1 M phosphate buffer (PB, pH 7.4). Brains were then removed and immersed in the same fixative for 2 hours or overnight at 4°C. Tissue blocks were washed thoroughly in 0.1 M PB. Coronal sections (60-μm thick) were cut using a vibratome (Leica V1000). Pre-embedding immunohistochemical analyses were performed as described previously[79]. Free-floating sections were incubated in 10% (v/v) normal goat serum (NGS) diluted in Tris-buffered saline (TBS). Sections were then incubated in 3-5 μg/mL diluted in TBS containing 1% (v/v) normal NGS, anti-$A_{2A}R$ [guinea pig anti-$A_{2A}R$ polyclonal (AB_2571656; Frontier Institute co., Japan)] or anti-A_1R [rabbit-anti-A_1R antibody (2 mg/ml; Affinity Bioreagents, Labome, USA)] antibodies, followed by incubation in goat anti-guinea pig IgG coupled to 1.4 nm gold or in goat anti-rabbit IgG coupled to 1.4 nm gold (Nanoprobes Inc., Stony Brook, NY, USA), respectively. Sections were postfixed in 1% (v/v) glutaraldehyde and washed in double-distilled water, followed by silver enhancement of the gold particles with an HQ Silver kit (Nanoprobes Inc.). Sections were then treated with osmium tetraoxide (1% in 0.1 m phosphate buffer), block-stained with uranyl acetate, dehydrated in a graded series of ethanol, and flat-embedded on glass slides in Durcupan (Fluka) resin. Regions of interest were cut at 70-90 nm on an ultramicrotome (Reichert Ultracut E, Leica, Austria) and collected on single-slot pioloform-coated copper grids. Staining was performed on 1% aqueous uranyl acetate drops followed by Reynolds's lead citrate. Ultrastructural analyses were performed in a Jeol-1010 electron microscope. Quantitative analysis of the relative abundance of $A_{2A}R$ or A_1R in the molecular layer of the dentate gyrus was performed from 60 μm coronal slices as described [79], in the area for MC-GC synapses and the area of PP-GC synapses. For each of the three animals, three tissue samples were obtained (nine total blocks). Electron microscopic serial ultrathin sections were cut close to the surface of each block because immunoreactivity decreased with depth. Randomly selected areas were captured at a final magnification of 45,000X, and measurements covered a total section area of ~5000 μm^2. Dendritic shafts, dendritic spines, and axon terminals were assessed for the presence of immunoparticles. The percentage of immunoparticles for $A_{2A}Rs$ or A_1Rs at postsynaptic and presynaptic sites was calculated. The perimeter of each axon terminal was measured in reference areas totaling ~2,000 μm^2. All axon terminals establishing excitatory synapses were counted and assessed from single ultrathin sections.

Two-photon live imaging of $GRAB_{Ado}$ in acute hippocampal slices— AAV_9.hSyn.GRAB.Ado1.0m (WZ Biosciences Inc) was injected (1 μL at 0.1 μL/min) unilaterally into the hilus of WT mice or *TrkB*$^{fl/fl}$ mice (3 - 4 weeks old). Slices were prepared 3 - 4 weeks post-injection, and the expression of GRABAdo1.0m was confirmed in MCs of the ipsilateral hippocampus of each injected mouse. Hippocampal slices from $GRAB_{Ado1.0m}$-injected mice were prepared using an ice-cold dissection buffer maintained in 5% CO_2/95% O_2 and containing (in mM): 25 $NaHCO_3$, 1.25 NaH_2PO_4, 2.5 KCl, 0.5 $CaCl_2$, 7 $MgCl_2$, 25 D-glucose, 110 choline chloride, 11.6 ascorbic acid, 3.1 pyruvic acid. Slices were transferred to 32°C ACSF for 30 min and kept at room temperature for at least 45 min before imaging. Slices were then transferred to an imaging chamber under an

Ultima 2-photon microscope (Bruker Corp.) equipped with a 60X NA 1.0 water-immersion objective and InSight DeepSee laser (Spectra-Physics). A 920-nm laser was used to excite $GRAB_{Ado1.0m}$, and the emission signal was acquired using a 525–570 nm band-pass filter. The field of view (512 X 512 pixels per frame) was chosen in the IML of contralateral hippocampal slices where MC commissural axons projected onto GCs and expressed $GRAB_{Ado1.0m}$. A broken tip stimulating patch-type micropipette filled with ACSF was positioned in the IML ~150 μm from the imaging region to activate MC axons. The region of interest (ROI) was magnified to 2X and at least 40 consecutive images (at 0.25 Hz) as a baseline using PrairieView 5.4 (Bruker Corp.). MC burst stimulation was applied after baseline acquisition, and at least 100 additional images (at 0.25 Hz) were acquired. To verify the reactivity of the ROI, adenosine (100 μM) was added at the end of the imaging session. The fluorescence intensity of the ROI was measured, and the $\Delta F/F_0$ of the $GRAB_{Ado1.0m}$ signal was calculated using ImageJ software. All recordings were performed at 28 ± 1 °C in a submersion-type recording chamber perfused at 2 mL/min with ACSF.

Seizure induction and monitoring—Epileptic seizures were induced acutely in 2-3–month-old mice. Intraperitoneal (i.p.) injections of 20-30 mg/kg of kainic acid (KA, HelloBio HB0355) prepared in saline solution the same day were performed. For behavioral seizure scoring, mice were monitored during the 120 min post-injection. Behavioral seizures were scored by an experimenter blind to condition (control *vs Adora2a* cKO), using a modified Racine scale as follows: stage 0: normal behavior, stage 1: immobility and rigidity, stage 2: head bobbing, stage 3: forelimb clonus and rearing, stage 4: continuous rearing and falling, stage 5: clonic-tonic seizure, stage 6: death. The maximum Racine score was recorded every 10 minutes, and the cumulative seizure score was obtained by summing these scores across all 12 bins of the 120-minute experiment.

Fiber photometry in freely behaving mice—AAV_9.hSyn.GRAB.Ado1.0m (1.2 μL at 0.1 μL/min) was unilaterally injected into the left DG (relative to bregma: 1.9 mm posterior, 1.25 mm lateral, 2.3 ventral) of *TrkB*$^{fl/fl}$ mice (5-6 week old). Contralaterally, AAV_5.CamKII.eGFP (control) or AAV_5.CamKII.GFP-CRE (*TrkB* cKO) was injected (0.5 μL at a flow rate of 0.1 μL/min) into the right DG (1.9 mm posterior, 1.25 mm lateral, 2.1 mm ventral). This allowed us to locally knockout *TrkB* from DG excitatory neurons. An optic fiber (200 μm diameter, NA = 0.37, Neurophotometrics) was then implanted unilaterally into the right DG above the IML (relative to bregma: 1.9 mm posterior, 1.25 mm lateral, 1.8 mm ventral) to record $GRAB_{Ado1.0m}$ fluorescence *in vivo* where *TrkB* was KO as compared to control. 3-5 weeks after surgery, the fluorescence signal was monitored before and after KA i.p. injection (30 mg/kg). To record $GRAB_{Ado1.0m}$ fluorescence, a three-channel multi-fiber photometry system (Neurophotometrics v1 Ltd) was used. 470 nm and 415 nm out-of-phase excitation lights were bandpass filtered and directed via a 20X objective (power: 30 μW). A single patch cord connected to the optic fiber implant was used to deliver light and collect the emitted fluorescence, which was filtered and projected on a CMOS camera sensor. The open-source software Bonsai was used for data acquisition (40 frames/s rate). The fluorescence intensity profile of each channel was calculated as the mean pixel value of the region of interest. To calculate $\Delta F/F_0$, the 470 nm-evoked signal was normalized by the isosbestic signal (415 nm) to correct for photobleaching and

potential artifacts. F_0 corresponds to the average of the last three minutes (baseline) before KA injection. The optic fiber location was verified *post hoc* to ensure that the fiber tip was in the ML of the DG. Animals with optic tips located outside of the DG or lacking AAV expression were excluded from the analysis. It is worth noting that the recording area is restricted to the vicinity (~200 μm) under the fiber tip[80].

Post-hoc analysis of AAV expression and optic fiber location—At the end of the experiments, viral expression and optic fiber location were verified post hoc (Figure 7). Mice were anesthetized with isoflurane (3-5%) and transcardially perfused with 4% paraformaldehyde (PFA) in 0.1 M sodium phosphate buffer (PBS). 50 μm-thick brain coronal sections were prepared using a DSK Microslicer (DTK-1000), stained with DAPI (1:1000) to label cell nuclei, and mounted with Prolong diamond antifade reagent montant (ThermoFisher) onto microscope slides. A Zeiss LSM 880 Airyscan Confocal microscope with Super-Resolution and ZEN (black edition) software and a 25X oil-immersion objective were used to acquire all images in this study.

Quantification and Statistical Analysis

The normality of distributions was assessed using the Shapiro-Wilk test. Student's unpaired and paired two-tailed t-tests were used in normal distributions to assess between-group and within-group differences, respectively. In unpaired t-tests, we checked for unequal variance. In cases where variance was unequal between normal distributions, we used a p-value that does not assume equal variance (Welch Correction). One-way ANOVA and One-way ANOVA repeated measure (RM) were used when more than two groups were compared. The non-parametric paired sample Wilcoxon signed rank test and Mann-Whitney's U test were used in non-normal distributions. Statistical significance was set to $p < 0.05$ (*** indicates $p < 0.001$, ** indicates $p < 0.01$, and * indicates $p < 0.05$). All values are reported as the mean ± SEM. Statistical results are summarized in Table S1. All experiments included at least three animals per condition. Statistical analysis was performed using OriginPro software (OriginLab).

Supplementary Material

Refer to Web version on PubMed Central for supplementary material.

Acknowledgments

We thank all Castillo lab members for their invaluable feedback. We thank Dr. Anita Autry (Einstein) for sharing her photometry system and for the technical support provided by her lab members, especially Ilaria Carta and Dr. Giovanni Podda., We thank Subrina Persaud for assisting with confocal image acquisition. We thank Dr. Yulong Li (Peking University) for helpful discussions about the adenosine sensor, Dr. Pascal Kaeser (Harvard University) for sharing an AAV-hSyn-Flex-ChIEF-TdTomato plasmid, and Dr. Lisa Monteggia (Vanderbilt University) for sharing *TrkB*$^{fl/fl}$ and *Bdnf*$^{fl/fl}$ mice, and Drs. Gaël Barthet and Christophe Mulle, Université de Bordeaux, for sharing the C1ql2 constructs. This work was supported by NIH grants R01 MH116673, R01MH125772, and R01 NS 113600 to P.E.C.. K.N. was partially supported by a Postdoctoral Research Fellowship (American Epilepsy Society), the Fondation pour la Recherche Médicale (postdoctoral fellowship for research abroad), and the Fondation Bettencourt Schueller (Prix pour les Jeunes Chercheurs 2016). C.B. was partially supported by a Postdoctoral Research Fellowship (American Epilepsy Society). Y.H. was supported by grants from JSPS KAKENHI (20H03358, 23H04240, and 23K18167). A.E.C. was partially supported by a Ruth L. Kirschstein Award (F32 NS071821), a NARSAD Young Investigator Grant from the Brain & Behavior Research Foundation, and by Chilean Fondecyt regular (#1201848). M.G. was supported by a Ruth L. Kirschstein Award (F31MH122134). R.L. was funded by the

Spanish MCIN/AEI/ 10.13039/501100011033 and by “ERDF A way of making Europe” (PID2021-125875OB-I00) and Junta de Comunidades de Castilla-La Mancha (SBPLY/21/180501/000064). Confocal images were obtained at the Einstein Imaging Core (supported by the Rose F. Kennedy Intellectual Disabilities Research Center - shared instrument grant 1S10OD25295 to Konstantin Dobrenis).

REFERENCES

1. Regehr WG, Carey MR, and Best AR (2009). Activity-dependent regulation of synapses by retrograde messengers. Neuron 63, 154–170. 10.1016/j.neuron.2009.06.021. [PubMed: 19640475]
2. Fitzsimonds RM, and Poo MM (1998). Retrograde signaling in the development and modification of synapses. Physiol Rev 78, 143–170. 10.1152/physrev.1998.78.1.143. [PubMed: 9457171]
3. Castillo PE (2012). Presynaptic LTP and LTD of excitatory and inhibitory synapses. Cold Spring Harb Perspect Biol 4. 10.1101/cshperspect.a005728.
4. Monday HR, Younts TJ, and Castillo PE (2018). Long-Term Plasticity of Neurotransmitter Release: Emerging Mechanisms and Contributions to Brain Function and Disease. Annu Rev Neurosci 41, 299–322. 10.1146/annurev-neuro-080317-062155. [PubMed: 29709205]
5. Davis GW, and Muller M (2015). Homeostatic control of presynaptic neurotransmitter release. Annu Rev Physiol 77, 251–270. 10.1146/annurev-physiol-021014-071740. [PubMed: 25386989]
6. Lisman JE (1999). Relating hippocampal circuitry to function: recall of memory sequences by reciprocal dentate-CA3 interactions. Neuron 22, 233–242. 10.1016/s0896-6273(00)81085-5. [PubMed: 10069330]
7. Scharfman HE (2016). The enigmatic mossy cell of the dentate gyrus. Nat Rev Neurosci 17, 562–575. 10.1038/nrn.2016.87. [PubMed: 27466143]
8. Jinde S, Zsiros V, and Nakazawa K (2013). Hilar mossy cell circuitry controlling dentate granule cell excitability. Front Neural Circuits 7, 14. 10.3389/fncir.2013.00014. [PubMed: 23407806]
9. Scharfman HE, and Myers CE (2012). Hilar mossy cells of the dentate gyrus: a historical perspective. Front Neural Circuits 6, 106. 10.3389/fncir.2012.00106. [PubMed: 23420672]
10. Ratzliff A, Santhakumar V, Howard A, and Soltesz I (2002). Mossy cells in epilepsy: rigor mortis or vigor mortis? Trends Neurosci 25, 140–144. 10.1016/s0166-2236(00)02122-6. [PubMed: 11852145]
11. Bui AD, Nguyen TM, Limouse C, Kim HK, Szabo GG, Felong S, Maroso M, and Soltesz I (2018). Dentate gyrus mossy cells control spontaneous convulsive seizures and spatial memory. Science 359, 787–790. 10.1126/science.aan4074. [PubMed: 29449490]
12. Botterill JJ, Lu YL, LaFrancois JJ, Bernstein HL, Alcantara-Gonzalez D, Jain S, Leary P, and Scharfman HE (2019). An Excitatory and Epileptogenic Effect of Dentate Gyrus Mossy Cells in a Mouse Model of Epilepsy. Cell Rep 29, 2875–2889 e2876. 10.1016/j.celrep.2019.10.100. [PubMed: 31775052]
13. Nasrallah K, Frechou MA, Yoon YJ, Persaud S, Goncalves JT, and Castillo PE (2022). Seizure-induced strengthening of a recurrent excitatory circuit in the dentate gyrus is proconvulsant. Proc Natl Acad Sci U S A 119, e2201151119. 10.1073/pnas.2201151119. [PubMed: 35930664]
14. Hashimotodani Y, Nasrallah K, Jensen KR, Chavez AE, Carrera D, and Castillo PE (2017). LTP at Hilar Mossy Cell-Dentate Granule Cell Synapses Modulates Dentate Gyrus Output by Increasing Excitation/Inhibition Balance. Neuron 95, 928–943 e923. 10.1016/j.neuron.2017.07.028. [PubMed: 28817805]
15. Berthoux C, Nasrallah K, Milner TA, and Castillo PE (2023). BDNF induces its own release to mediate presynaptic plasticity. bioRxiv 10.1101/2021.12.30.474558.
16. Younts TJ, Chevaleyre V, and Castillo PE (2013). CA1 pyramidal cell theta-burst firing triggers endocannabinoid-mediated long-term depression at both somatic and dendritic inhibitory synapses. J Neurosci 33, 13743–13757. 10.1523/JNEUROSCI.0817-13.2013. [PubMed: 23966696]
17. Lysetskiy M, Foldy C, and Soltesz I (2005). Long- and short-term plasticity at mossy fiber synapses on mossy cells in the rat dentate gyrus. Hippocampus 15, 691–696. 10.1002/hipo.20096. [PubMed: 15986406]

18. Chiu CQ, and Castillo PE (2008). Input-specific plasticity at excitatory synapses mediated by endocannabinoids in the dentate gyrus. Neuropharmacology 54, 68–78. 10.1016/j.neuropharm.2007.06.026. [PubMed: 17706254]
19. Shimojo M, Courchet J, Pieraut S, Torabi-Rander N, Sando R 3rd, Polleux F, and Maximov A (2015). SNAREs Controlling Vesicular Release of BDNF and Development of Callosal Axons. Cell Rep 11, 1054–1066. 10.1016/j.celrep.2015.04.032. [PubMed: 25959820]
20. Barthet G, Jorda-Siquier T, Rumi-Masante J, Bernadou F, Muller U, and Mulle C (2018). Presenilin-mediated cleavage of APP regulates synaptotagmin-7 and presynaptic plasticity. Nat Commun 9, 4780. 10.1038/s41467-018-06813-x. [PubMed: 30429473]
21. Monday HR, Kharod SC, Yoon YJ, Singer RH, and Castillo PE (2022). Presynaptic FMRP and local protein synthesis support structural and functional plasticity of glutamatergic axon terminals. Neuron 110, 2588–2606 e2586. 10.1016/j.neuron.2022.05.024. [PubMed: 35728596]
22. Jensen KR, Berthoux C, Nasrallah K, and Castillo PE (2021). Multiple cannabinoid signaling cascades powerfully suppress recurrent excitation in the hippocampus. Proc Natl Acad Sci U S A 118. 10.1073/pnas.2017590118.
23. Williams JH, Li YG, Nayak A, Errington ML, Murphy KP, and Bliss TV (1993). The suppression of long-term potentiation in rat hippocampus by inhibitors of nitric oxide synthase is temperature and age dependent. Neuron 11, 877–884. 10.1016/0896-6273(93)90117-a. [PubMed: 7694601]
24. Normandin M, Gagne J, Bernard J, Elie R, Miceli D, Baudry M, and Massicotte G (1996). Involvement of the 12-lipoxygenase pathway of arachidonic acid metabolism in homosynaptic long-term depression of the rat hippocampus. Brain Res 730, 40–46. 10.1016/0006-8993(96)00428-3. [PubMed: 8883886]
25. Chevaleyre V, and Castillo PE (2003). Heterosynaptic LTD of hippocampal GABAergic synapses: a novel role of endocannabinoids in regulating excitability. Neuron 38, 461–472. 10.1016/s0896-6273(03)00235-6. [PubMed: 12741992]
26. Sebastiao AM, and Ribeiro JA (2009). Triggering neurotrophic factor actions through adenosine A2A receptor activation: implications for neuroprotection. Br J Pharmacol 158, 15–22. 10.1111/j.1476-5381.2009.00157.x. [PubMed: 19508402]
27. Diogenes MJ, Fernandes CC, Sebastiao AM, and Ribeiro JA (2004). Activation of adenosine A2A receptor facilitates brain-derived neurotrophic factor modulation of synaptic transmission in hippocampal slices. J Neurosci 24, 2905–2913. 10.1523/JNEUROSCI.4454-03.2004. [PubMed: 15044529]
28. Fontinha BM, Diogenes MJ, Ribeiro JA, and Sebastiao AM (2008). Enhancement of long-term potentiation by brain-derived neurotrophic factor requires adenosine A2A receptor activation by endogenous adenosine. Neuropharmacology 54, 924–933. 10.1016/j.neuropharm.2008.01.011. [PubMed: 18384819]
29. Latini S, and Pedata F (2001). Adenosine in the central nervous system: release mechanisms and extracellular concentrations. J Neurochem 79, 463–484. 10.1046/j.1471-4159.2001.00607.x. [PubMed: 11701750]
30. King AE, Ackley MA, Cass CE, Young JD, and Baldwin SA (2006). Nucleoside transporters: from scavengers to novel therapeutic targets. Trends Pharmacol Sci 27, 416–425. 10.1016/j.tips.2006.06.004. [PubMed: 16820221]
31. Lovatt D, Xu Q, Liu W, Takano T, Smith NA, Schnermann J, Tieu K, and Nedergaard M (2012). Neuronal adenosine release, and not astrocytic ATP release, mediates feedback inhibition of excitatory activity. Proc Natl Acad Sci U S A 109, 6265–6270. 10.1073/pnas.1120997109. [PubMed: 22421436]
32. Wall MJ, and Dale N (2013). Neuronal transporter and astrocytic ATP exocytosis underlie activity-dependent adenosine release in the hippocampus. J Physiol 591, 3853–3871. 10.1113/jphysiol.2013.253450. [PubMed: 23713028]
33. Pons-Bennaceur A, Tsintsadze V, Bui TT, Tsintsadze T, Minlebaev M, Milh M, Scavarda D, Giniatullin R, Giniatullina R, Shityakov S, et al. (2019). Diadenosine-Polyphosphate Analogue AppCH2ppA Suppresses Seizures by Enhancing Adenosine Signaling in the Cortex. Cereb Cortex 29, 3778–3795. 10.1093/cercor/bhy257. [PubMed: 30295710]

34. Tabuchi E, Sakaba T, and Hashimotodani Y (2022). Excitatory selective LTP of supramammillary glutamatergic/GABAergic cotransmission potentiates dentate granule cell firing. Proc Natl Acad Sci U S A 119, e2119636119. 10.1073/pnas.2119636119. [PubMed: 35333647]
35. Harris TE, Persaud SJ, and Jones PM (1997). Pseudosubstrate inhibition of cyclic AMP-dependent protein kinase in intact pancreatic islets: effects on cyclic AMP-dependent and glucose-dependent insulin secretion. Biochem Biophys Res Commun 232, 648–651. 10.1006/bbrc.1997.6344. [PubMed: 9126329]
36. Skeberdis VA, Chevaleyre V, Lau CG, Goldberg JH, Pettit DL, Suadicani SO, Lin Y, Bennett MV, Yuste R, Castillo PE, and Zukin RS (2006). Protein kinase A regulates calcium permeability of NMDA receptors. Nat Neurosci 9, 501–510. 10.1038/nn1664. [PubMed: 16531999]
37. Atwood BK, Lovinger DM, and Mathur BN (2014). Presynaptic long-term depression mediated by Gi/o-coupled receptors. Trends Neurosci 37, 663–673. 10.1016/j.tins.2014.07.010. [PubMed: 25160683]
38. Quiroz C, Lujan R, Uchigashima M, Simoes AP, Lerner TN, Borycz J, Kachroo A, Canas PM, Orru M, Schwarzschild MA, et al. (2009). Key modulatory role of presynaptic adenosine A2A receptors in cortical neurotransmission to the striatal direct pathway. ScientificWorldJournal 9, 1321–1344. 10.1100/tsw.2009.143. [PubMed: 19936569]
39. Buckmaster PS, Wenzel HJ, Kunkel DD, and Schwartzkroin PA (1996). Axon arbors and synaptic connections of hippocampal mossy cells in the rat in vivo. J Comp Neurol 366, 271–292. 10.1002/(sici)1096-9861(19960304)366:2<270::aid-cne7>3.0.co;2-2. [PubMed: 8698887]
40. Arch JR, and Newsholme EA (1978). Activities and some properties of 5'-nucleotidase, adenosine kinase and adenosine deaminase in tissues from vertebrates and invertebrates in relation to the control of the concentration and the physiological role of adenosine. Biochem J 174, 965–977. 10.1042/bj1740965. [PubMed: 215126]
41. Peng W, Wu Z, Song K, Zhang S, Li Y, and Xu M (2020). Regulation of sleep homeostasis mediator adenosine by basal forebrain glutamatergic neurons. Science 369. 10.1126/science.abb0556.
42. Wu Z, Cui Y, Wang H, Wu H, Wan Y, Li B, Wang L, Pan S, Peng W, Dong A, et al. (2023). Neuronal activity-induced, equilibrative nucleoside transporter-dependent, somatodendritic adenosine release revealed by a GRAB sensor. Proc Natl Acad Sci U S A 120, e2212387120. 10.1073/pnas.2212387120. [PubMed: 36996110]
43. Henze DA, Wittner L, and Buzsaki G (2002). Single granule cells reliably discharge targets in the hippocampal CA3 network in vivo. Nat Neurosci 5, 790–795. 10.1038/nn887. [PubMed: 12118256]
44. Pernia-Andrade AJ, and Jonas P (2014). Theta-gamma-modulated synaptic currents in hippocampal granule cells in vivo define a mechanism for network oscillations. Neuron 81, 140–152. 10.1016/j.neuron.2013.09.046. [PubMed: 24333053]
45. Diamantaki M, Frey M, Berens P, Preston-Ferrer P, and Burgalossi A (2016). Sparse activity of identified dentate granule cells during spatial exploration. Elife 5. 10.7554/eLife.20252.
46. GoodSmith D, Chen X, Wang C, Kim SH, Song H, Burgalossi A, Christian KM, and Knierim JJ (2017). Spatial Representations of Granule Cells and Mossy Cells of the Dentate Gyrus. Neuron 93, 677–690 e675. 10.1016/j.neuron.2016.12.026. [PubMed: 28132828]
47. Senzai Y, and Buzsaki G (2017). Physiological Properties and Behavioral Correlates of Hippocampal Granule Cells and Mossy Cells. Neuron 93, 691–704 e695. 10.1016/j.neuron.2016.12.011. [PubMed: 28132824]
48. Danielson NB, Turi GF, Ladow M, Chavlis S, Petrantonakis PC, Poirazi P, and Losonczy A (2017). In Vivo Imaging of Dentate Gyrus Mossy Cells in Behaving Mice. Neuron 93, 552–559 e554. 10.1016/j.neuron.2016.12.019. [PubMed: 28132825]
49. Leschik J, Eckenstaler R, Endres T, Munsch T, Edelmann E, Richter K, Kobler O, Fischer KD, Zuschratter W, Brigadski T, et al. (2019). Prominent Postsynaptic and Dendritic Exocytosis of Endogenous BDNF Vesicles in BDNF-GFP Knock-in Mice. Mol Neurobiol 56, 6833–6855. 10.1007/s12035-019-1551-0. [PubMed: 30929164]

50. Ribeiro JA, and Sebastiao AM (1987). On the role, inactivation and origin of endogenous adenosine at the frog neuromuscular junction. J Physiol 384, 571–585. 10.1113/jphysiol.1987.sp016470. [PubMed: 2821240]
51. Zimmermann H. (2006). Ectonucleotidases in the nervous system. Novartis Found Symp 276, 113–128; discussion 128-130, 233-117, 275-181. [PubMed: 16805426]
52. Wall M, and Dale N (2008). Activity-dependent release of adenosine: a critical re-evaluation of mechanism. Curr Neuropharmacol 6, 329–337. 10.2174/157015908787386087. [PubMed: 19587854]
53. Lee FS, and Chao MV (2001). Activation of Trk neurotrophin receptors in the absence of neurotrophins. Proc Natl Acad Sci U S A 98, 3555–3560. 10.1073/pnas.061020198. [PubMed: 11248116]
54. Rodrigues TM, Jeronimo-Santos A, Sebastiao AM, and Diogenes MJ (2014). Adenosine A(2A) Receptors as novel upstream regulators of BDNF-mediated attenuation of hippocampal Long-Term Depression (LTD). Neuropharmacology 79, 389–398. 10.1016/j.neuropharm.2013.12.010. [PubMed: 24361450]
55. Ribeiro FF, Ferreira F, Rodrigues RS, Soares R, Pedro DM, Duarte-Samartinho M, Aroeira RI, Ferreiro E, Valero J, Sola S, et al. (2021). Regulation of hippocampal postnatal and adult neurogenesis by adenosine A(2A) receptor: Interaction with brain-derived neurotrophic factor. Stem Cells 39, 1362–1381. 10.1002/stem.3421. [PubMed: 34043863]
56. Correia-de-Sa P, Sebastiao AM, and Ribeiro JA (1991). Inhibitory and excitatory effects of adenosine receptor agonists on evoked transmitter release from phrenic nerve ending of the rat. Br J Pharmacol 103, 1614–1620. 10.1111/j.1476-5381.1991.tb09836.x. [PubMed: 1679362]
57. Pousinha PA, Diogenes MJ, Ribeiro JA, and Sebastiao AM (2006). Triggering of BDNF facilitatory action on neuromuscular transmission by adenosine A2A receptors. Neurosci Lett 404, 143–147. 10.1016/j.neulet.2006.05.036. [PubMed: 16790314]
58. Dixon AK, Gubitz AK, Sirinathsinghji DJ, Richardson PJ, and Freeman TC (1996). Tissue distribution of adenosine receptor mRNAs in the rat. Br J Pharmacol 118, 1461–1468. 10.1111/j.1476-5381.1996.tb15561.x. [PubMed: 8832073]
59. Dias RB, Rombo DM, Ribeiro JA, Henley JM, and Sebastiao AM (2013). Adenosine: setting the stage for plasticity. Trends Neurosci 36, 248–257. 10.1016/j.tins.2012.12.003. [PubMed: 23332692]
60. Duster R, Prickaerts J, and Blokland A (2014). Purinergic signaling and hippocampal long-term potentiation. Curr Neuropharmacol 12, 37–43. 10.2174/1570159X113119990045. [PubMed: 24533014]
61. Kase H. (2001). New aspects of physiological and pathophysiological functions of adenosine A2A receptor in basal ganglia. Biosci Biotechnol Biochem 65, 1447–1457. 10.1271/bbb.65.1447. [PubMed: 11515525]
62. Pousinha PA, Correia AM, Sebastiao AM, and Ribeiro JA (2010). Predominance of adenosine excitatory over inhibitory effects on transmission at the neuromuscular junction of infant rats. J Pharmacol Exp Ther 332, 153–163. 10.1124/jpet.109.157255. [PubMed: 19789361]
63. Correia-de-Sa P, Timoteo MA, and Ribeiro JA (1996). Presynaptic A1 inhibitory/A2A facilitatory adenosine receptor activation balance depends on motor nerve stimulation paradigm at the rat hemidiaphragm. J Neurophysiol 76, 3910–3919. 10.1152/jn.1996.76.6.3910. [PubMed: 8985888]
64. Sebastiao AM, and Ribeiro JA (2009). Adenosine receptors and the central nervous system. Handb Exp Pharmacol, 471–534. 10.1007/978-3-540-89615-9_16. [PubMed: 19639292]
65. Alzheimer C, Rohrenbeck J, and ten Bruggencate G (1991). Adenosine depresses induction of LTP at the mossy fiber-CA3 synapse in vitro. Brain Res 543, 163–165. 10.1016/0006-8993(91)91061-5. [PubMed: 2054670]
66. Forghani R, and Krnjevic K (1995). Adenosine antagonists have differential effects on induction of long-term potentiation in hippocampal slices. Hippocampus 5, 71–77. 10.1002/hipo.450050109. [PubMed: 7787948]
67. Fredes F, Silva MA, Koppensteiner P, Kobayashi K, Joesch M, and Shigemoto R (2021). Ventro-dorsal Hippocampal Pathway Gates Novelty-Induced Contextual Memory Formation. Curr Biol 31, 25–38 e25. 10.1016/j.cub.2020.09.074. [PubMed: 33065009]

68. Fontinha BM, Delgado-Garcia JM, Madronal N, Ribeiro JA, Sebastiao AM, and Gruart A (2009). Adenosine A(2A) receptor modulation of hippocampal CA3-CA1 synapse plasticity during associative learning in behaving mice. Neuropsychopharmacology 34, 1865–1874. 10.1038/npp.2009.8. [PubMed: 19212319]
69. Wei CJ, Augusto E, Gomes CA, Singer P, Wang Y, Boison D, Cunha RA, Yee BK, and Chen JF (2014). Regulation of fear responses by striatal and extrastriatal adenosine A2A receptors in forebrain. Biol Psychiatry 75, 855–863. 10.1016/j.biopsych.2013.05.003. [PubMed: 23820821]
70. Beamer E, Kuchukulla M, Boison D, and Engel T (2021). ATP and adenosine-Two players in the control of seizures and epilepsy development. Prog Neurobiol 204, 102105. 10.1016/j.pneurobio.2021.102105. [PubMed: 34144123]
71. El Yacoubi M, Ledent C, Parmentier M, Costentin J, and Vaugeois JM (2008). Evidence for the involvement of the adenosine A(2A) receptor in the lowered susceptibility to pentylenetetrazol-induced seizures produced in mice by long-term treatment with caffeine. Neuropharmacology 55, 35–40. 10.1016/j.neuropharm.2008.04.007. [PubMed: 18486156]
72. El Yacoubi M, Ledent C, Parmentier M, Costentin J, and Vaugeois JM (2009). Adenosine A2A receptor deficient mice are partially resistant to limbic seizures. Naunyn Schmiedebergs Arch Pharmacol 380, 223–232. 10.1007/s00210-009-0426-8. [PubMed: 19488739]
73. Jones PA, Smith RA, and Stone TW (1998). Protection against hippocampal kainate excitotoxicity by intracerebral administration of an adenosine A2A receptor antagonist. Brain Res 800, 328–335. 10.1016/s0006-8993(98)00540-x. [PubMed: 9685693]
74. Lee HK, Choi SS, Han KJ, Han EJ, and Suh HW (2004). Roles of adenosine receptors in the regulation of kainic acid-induced neurotoxic responses in mice. Brain Res Mol Brain Res 125, 76–85. 10.1016/j.molbrainres.2004.03.004. [PubMed: 15193424]
75. Rosim FE, Persike DS, Nehlig A, Amorim RP, de Oliveira DM, and Fernandes MJ (2011). Differential neuroprotection by A(1) receptor activation and A(2A) receptor inhibition following pilocarpine-induced status epilepticus. Epilepsy Behav 22, 207–213. 10.1016/j.yebeh.2011.07.004. [PubMed: 21852200]
76. Fukuda M, Suzuki Y, Hino H, Morimoto T, and Ishii E (2011). Activation of central adenosine A(2A) receptors lowers the seizure threshold of hyperthermia-induced seizure in childhood rats. Seizure 20, 156–159. 10.1016/j.seizure.2010.11.012. [PubMed: 21144776]
77. Sandau US, Colino-Oliveira M, Jones A, Saleumvong B, Coffman SQ, Liu L, Miranda-Lourenco C, Palminha C, Batalha VL, Xu Y, et al. (2016). Adenosine Kinase Deficiency in the Brain Results in Maladaptive Synaptic Plasticity. J Neurosci 36, 12117–12128. 10.1523/JNEUROSCI.2146-16.2016. [PubMed: 27903722]
78. McNamara JO, and Scharfman HE (2012). Temporal Lobe Epilepsy and the BDNF Receptor, TrkB. In Jasper's Basic Mechanisms of the Epilepsies, th, Noebels JL, Avoli M, Rogawski MA, Olsen RW, and Delgado-Escueta AV, eds.
79. Lujan R, Nusser Z, Roberts JD, Shigemoto R, and Somogyi P (1996). Perisynaptic location of metabotropic glutamate receptors mGluR1 and mGluR5 on dendrites and dendritic spines in the rat hippocampus. Eur J Neurosci 8, 1488–1500. 10.1111/j.1460-9568.1996.tb01611.x. [PubMed: 8758956]
80. Pisano F, Pisanello M, Lee SJ, Lee J, Maglie E, Balena A, Sileo L, Spagnolo B, Bianco M, Hyun M, et al. (2019). Depth-resolved fiber photometry with a single tapered optical fiber implant. Nat Methods 16, 1185–1192. 10.1038/s41592-019-0581-x. [PubMed: 31591577]

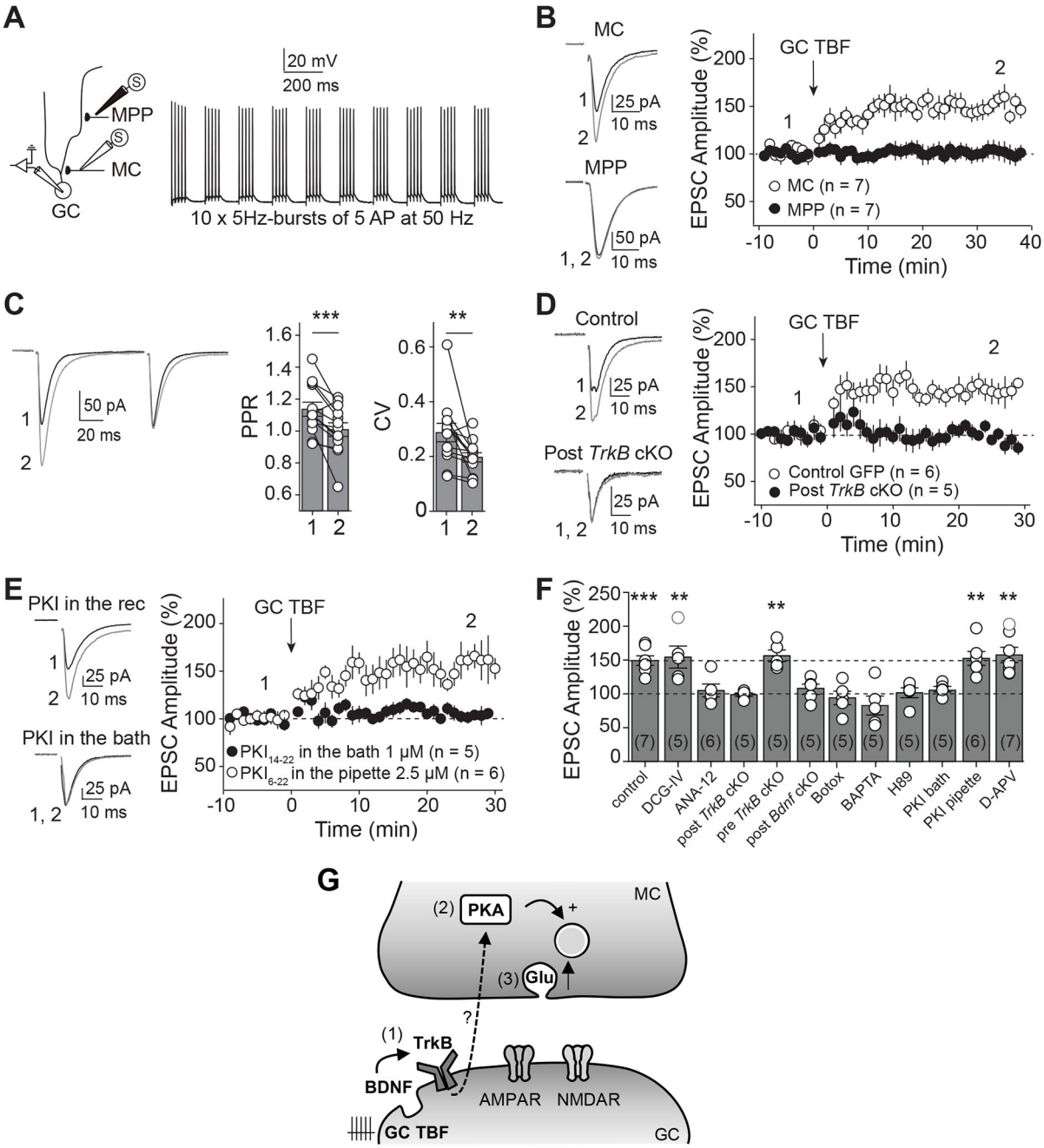

Figure 1: Theta-burst firing of a single GC induces presynaptic LTP at the MC-GC synapse

(A) *Left,* Diagram illustrating the recording configuration. MC and MPP EPSCs were recorded from the same GC and evoked with stimulation electrodes placed in the inner and middle molecular layer, respectively. *Right*, Current clamp recording showing GC theta-burst firing (GC TBF). LTP induction protocol (GC TBF) was composed of 10 bursts at 5 Hz of 5 action potentials at 50 Hz, repeated 4 times every 5 s.

(B) *Left,* Representative traces before (1) and after (2) GC TBF delivery. *Right,* Time-course plot showing that GC TBF induced LTP at MC-GC but not at MPP-GC synapses.

(C) GC TBF-induced LTP was associated with significant reduction in PPR and CV (n = 13 cells). ** $p < 0.01$, *** $p < 0.001$.

(D) LTP was abolished when TrkB was conditionally knocked out from from GCs (Post *TrkB* cKO, $TrkB^{fl/fl}$ mice injected in the dorsal blade with AAV_5.CaMKII.Cre.GFP). LTP was unaffected in control animals (Control, $TrkB^{fl/fl}$ mice injected in the dorsal blade with AAV_5.CaMKII.eGFP).

(E) LTP was normally induced when loading PKI_{6-22} (2.5 μM) in GCs via the recording pipette but completely blocked when the cell-permeable PKA inhibitor PKI_{14-22} myristoylated (1 μM) was bath applied.

(F) Summary bar graph showing the magnitude of GC TBF-induced LTP in the presence of DGC-IV (1 μM), when TrkB was conditionally knocked out from MCs (Pre *TrkB* cKO), when loading the PKI_{6-22} (2.5 μM) in GCs, and in the presence of D-APV (50 μM). LTP was abolished in the presence of the TrkB antagonist ANA-12 (15 μM), when Botox (0.5 μM) was loaded postsynaptically, in postsynaptic BDNF and *TrkB* cKO mice, and during bath application of the PKA inhibitors H89 (10 μM) or myristoylated PKI_{14-22} μM). Time-course summary plots are shown in Figure S1. ** $p < 0.01$, *** $p < 0.001$.

(G) Scheme illustrating the emerging model for the mechanism underlying GC TBF-LTP. GC TBF triggers postsynaptic BDNF release and subsequent TrkB activation in GCs (1). Presynaptic PKA is then engaged downstream of postsynaptic BDNF/TrkB signaling (2), suggesting the requirement of a retrograde signal. Lastly, presynaptic PKA activation resulted in a long-lasting increase in glutamate release (3).

Numbers in parentheses indicate the number of cells. Data are presented as mean ± SEM.

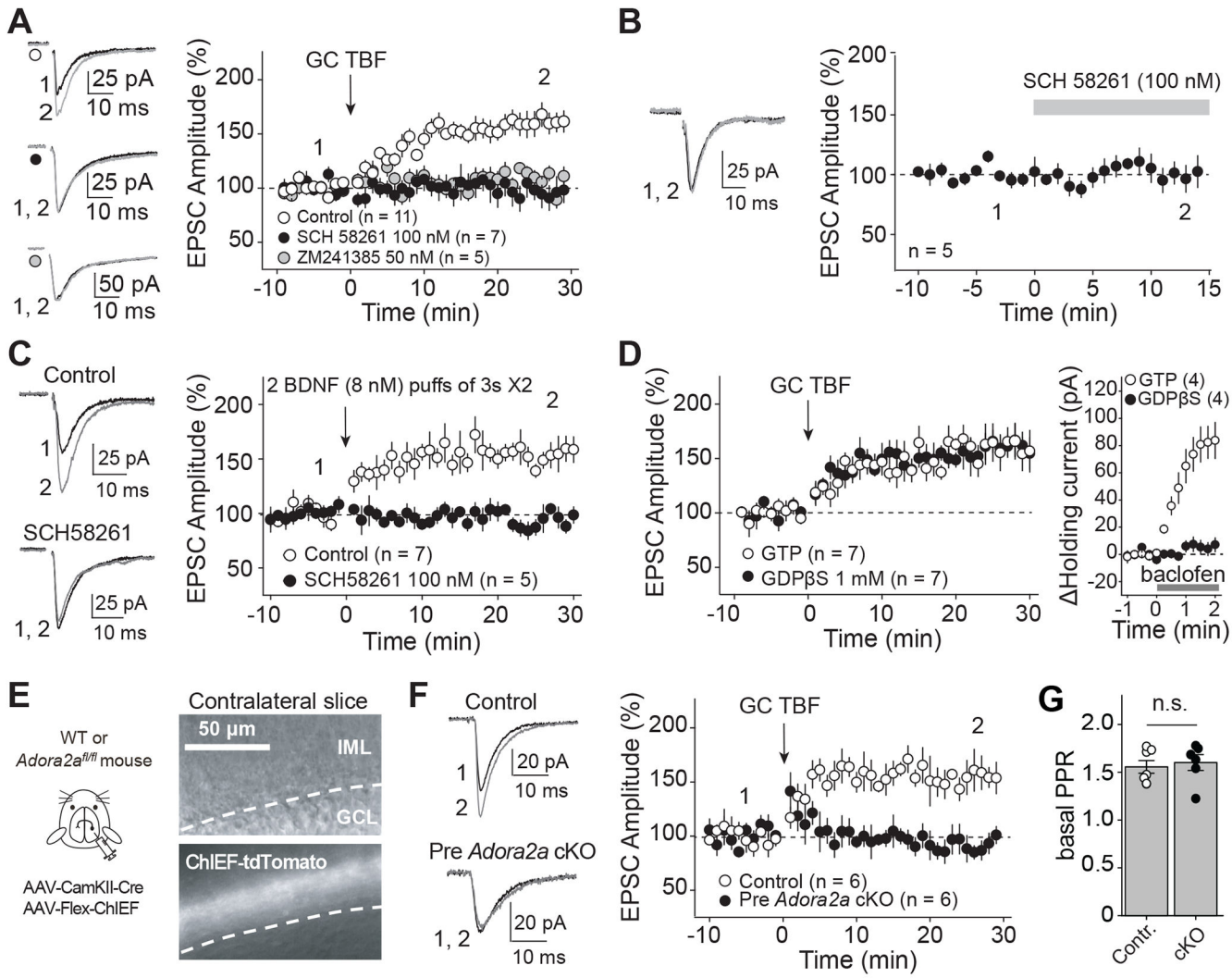

Figure 2: MC-GC LTP requires activation of presynaptic A_{2A}Rs

(A) Bath application of the A_{2A}R selective antagonists SCH 58261 (100 nM) and ZM241385 (50 nM) blocked GC TBF-induced LTP.

(B) SCH 58261 (100 nM) did not change basal EPSC amplitude.

(C) SCH 58261 (100 nM) abolished LTP induced by BDNF puffs (8 nM, 2 puffs of 3 s in the IML), as compared with interleaved controls.

(D) *Left,* loading GDPβS in the recording pipette did not affect TBF-induced LTP. *Right,* interleaved, positive control showing that replacing GTP by 1 mM GDPβS in the internal solution efficiently abolished the $GABA_B$ receptor agonist (baclofen, 10 µM)-induced increase in holding current.

(E) *Left,* A mix of AAV_5.CamKII. Cre-mCherry and AAV_{DJ}.hSyn.Flex.ChIEF.Tdtomato was injected unilaterally into the DG of *Adora2a*$^{fl/fl}$ (cKO) or WT (control) mice. *Right,* Infrared/differential interference contrast (IR/DIC, top) and fluorescence (bottom) images show that ChIEF-TdTomato was selectively expressed in putative MC axons of contralateral IML.

(F) Light-evoked MC EPSCs were recorded in contralateral DG. MC-GC LTP was abolished in presynaptic *Adora2a* conditional knockout mice as compared with controls.
(G) Basal PPR was similar in control and presynaptic *Adora2a* cKO animals, n.s. $p > 0.05$., Numbers in parentheses represent number of cells. Data are presented as mean ± SEM.

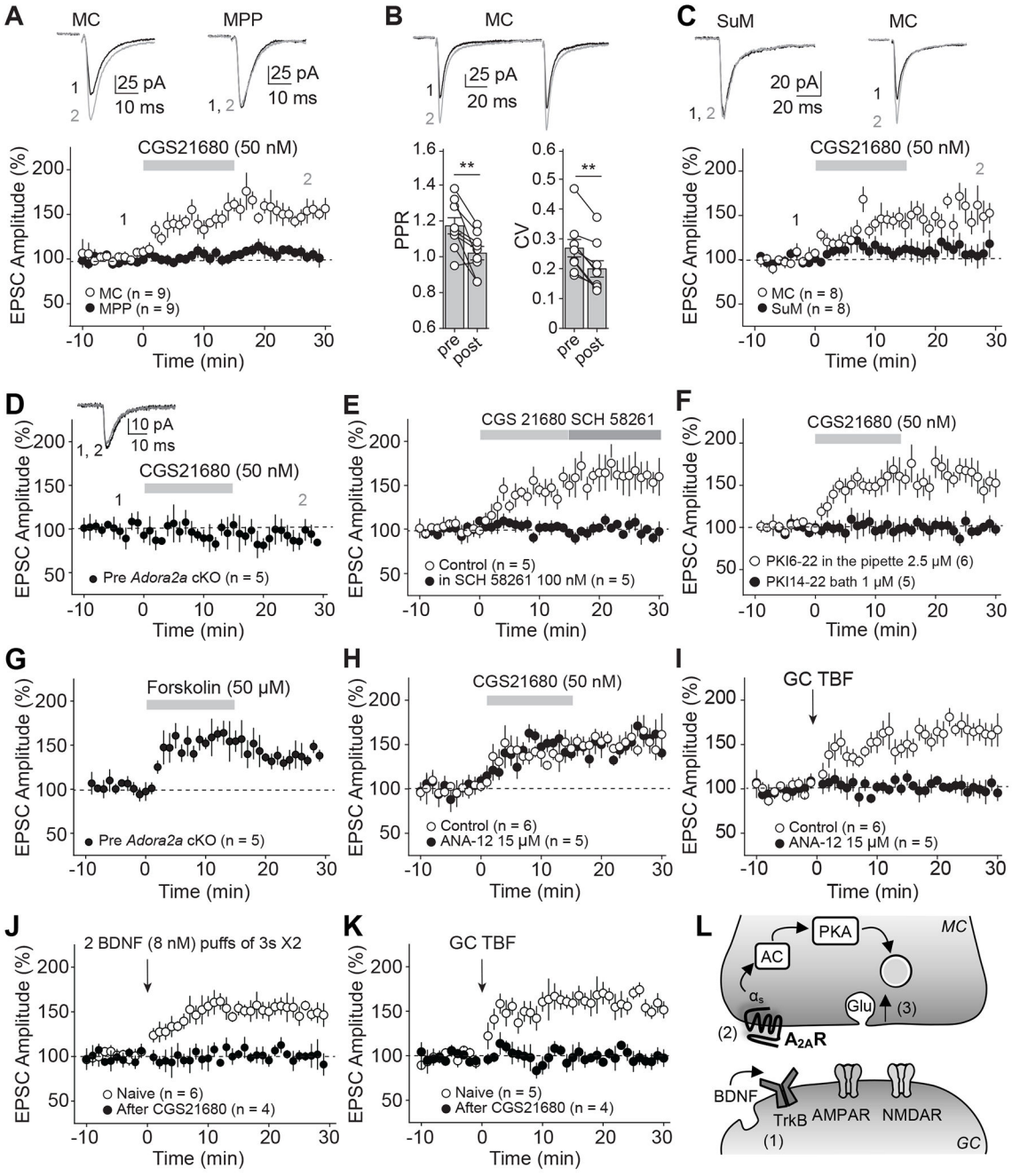

Figure 3: $A_{2A}R$ activation is sufficient to trigger PKA-dependent LTP at MC-GC but not at MPP-GC synapses.

(A) Representative traces *(top)* and time-course summary plot *(bottom)* showing that bath application of the $A_{2A}R$ selective agonist CGS21680 (50 nM) potentiated MC-GC but not MPP-GC synaptic transmission.

(B) CGS21680-induced potentiation at MC-GC synapse was associated with a significant reduction of both PPR and CV. ** $p < 0.01$; n = 9 cells.

(C) AAV1-EF1a-DIO-hChR2(H134R)-eYFP was injected into the SuM of VGluT2-Cre mice. Light-evoked SuM EPSCs and electrically-triggered MC EPSCs were monitored in GCs. CGS21680 (50 nM) potentiated MC-GC but not SuM-GC synaptic transmission.
(D) CGS21680-induced potentiation was abolished in presynaptic *Adora2a* cKO mice. A mix of AAV_{5}.CamKII.Cre-mCherry and AAV_{DJ}.hSyn.Flex.ChIEF.TdTomato was injected unilaterally into the DG of *Adora2a*$^{fl/fl}$. Light-evoked MC EPSCs were recorded in contralateral DG.
(E) CGS21680 induced long-lasting potentiation even when the $A_{2A}R$ selective antagonist SCH 58261 (100 nM)was included during CGS21680 washout. CGS21680-induced LTP was completely abolished in continuous presence of SCH 58261.
(F) Loading the selective PKA blocker PKI_{6-22} (2.5 μM) in GCs via the recording pipette did not impair CGS21680-induced LTP while bath application of the cell-permeable PKA inhibitor PKI_{14-22} myristoylated (1 μM) completely blocked LTP.
(G) Light-evoked MC EPSCs showing that bath application of the adenylyl cyclase activator forskolin (50 μM) induced LTP in presynaptic *Adora2a* cKO mice.
(H) Bath application of the TrkB antagonist ANA-12 (15 μM) did not impair CGS21680-induced LTP.
(I) Positive control in interleaved experiments showing that ANA-12 (15 μM) efficiently blocked GC TBF-induced LTP.
(J, K) Bath application of CGS21680 (50 nM, 15 min) occluded LTP induced with both BDNF (8 nM, 2 puffs of 3 s in the IML, J) and GC TBF (K).
(L) Cartoon illustrating how activation of presynaptic $A_{2A}Rs$ induces PKA-dependent long-lasting increase in glutamate (Glu) release. The presynaptic $A_{2A}R$/PKA pathway is engaged downstream of postsynaptic BDNF/TrkB signaling during LTP induction.
Numbers in parentheses represent number of cells. Data are presented as mean ± SEM.

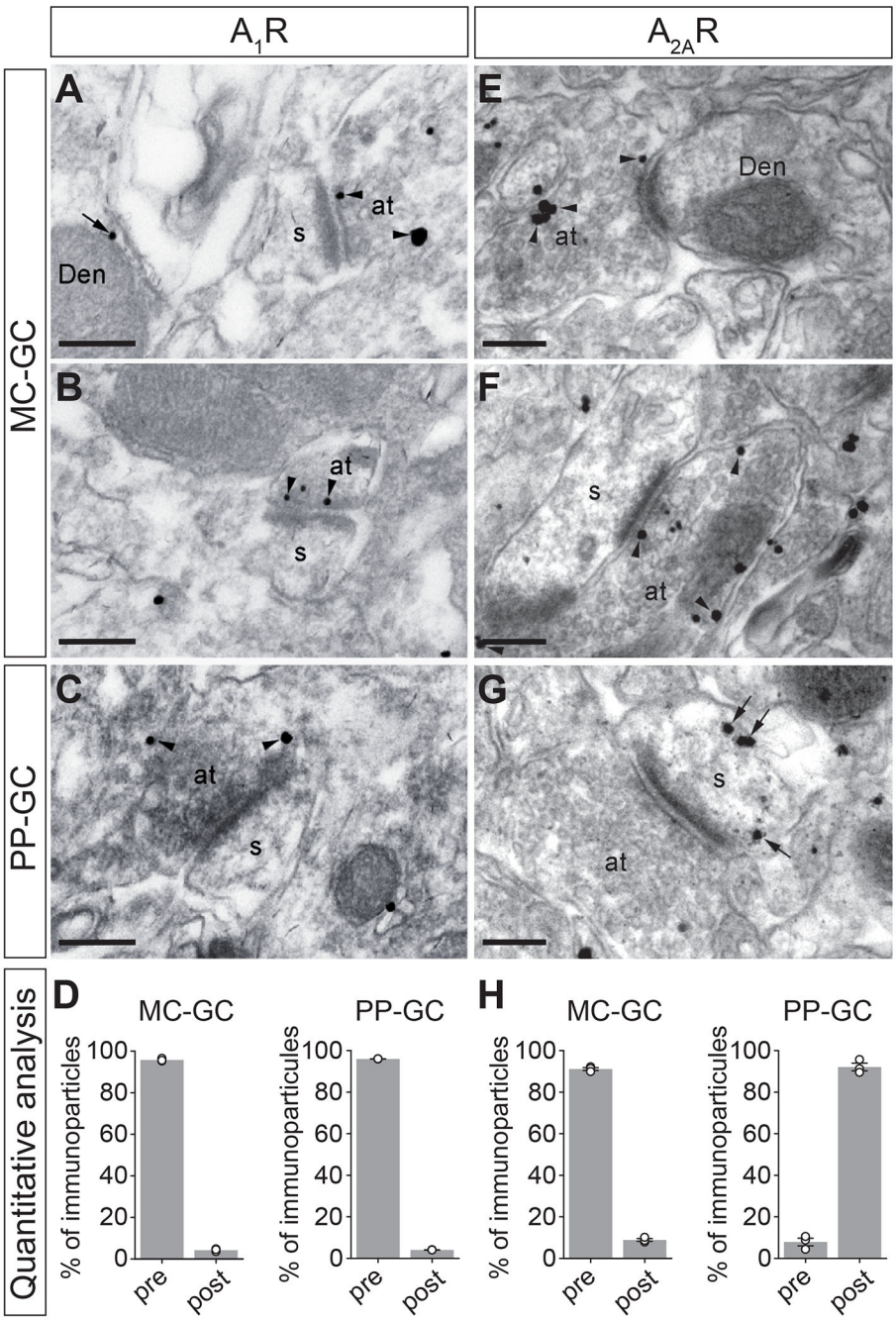

Figure 4: Subcellular localization of A_1 and A_{2A} receptors in the molecular layer of the dentate gyrus.

(A-C, E-G) Electron micrographs of the molecular layer of the dentate gyrus showing immunoreactivity for A_1Rs and A_{2A}Rs revealed by pre-embedding immunogold methods. **(A-C)** Both at MC-GC **(A, B)** and PP-GC **(C)** putative synapses, immunoparticles for A_1R were mainly observed on the presynaptic plasma membrane (arrowheads) of axon terminals (at), with very low frequency in postsynaptic sites (arrows) of spines (s) or dendritic shafts (Den).

(D) Quantitative analysis of the relative number of immunoparticles found in the presynaptic membrane for A_1R at MC-GC and MPP-GC putative synapses. From the total number of immunoparticles detected (n = 490 for MC-GC; n = 419 for MPP-GC synapses, N = 3 mice), 468 (95.5%) and 402 (95.9%) were present in presynaptic sites of MC-GC and MPP-GC putative synapses, respectively.

(E-H) Electron micrographs **(E-G)** and quantitative analysis **(H)** showing that, at putative MC-GC synapses **(E, F** and **H)**, immunoparticles for $A_{2A}R$ were mainly detected presynaptically (91.0%) whereas they were mainly found on the postsynaptic plasma membrane (92.0%) of putative PP-GC synapses **(G, H)**. Total number of immunoparticles: n = 668 for MC-GC; n = 690 for MPP-GC synapses, N = 3 mice.

Scale bars: 200 nm. Data are presented as mean ± SEM.

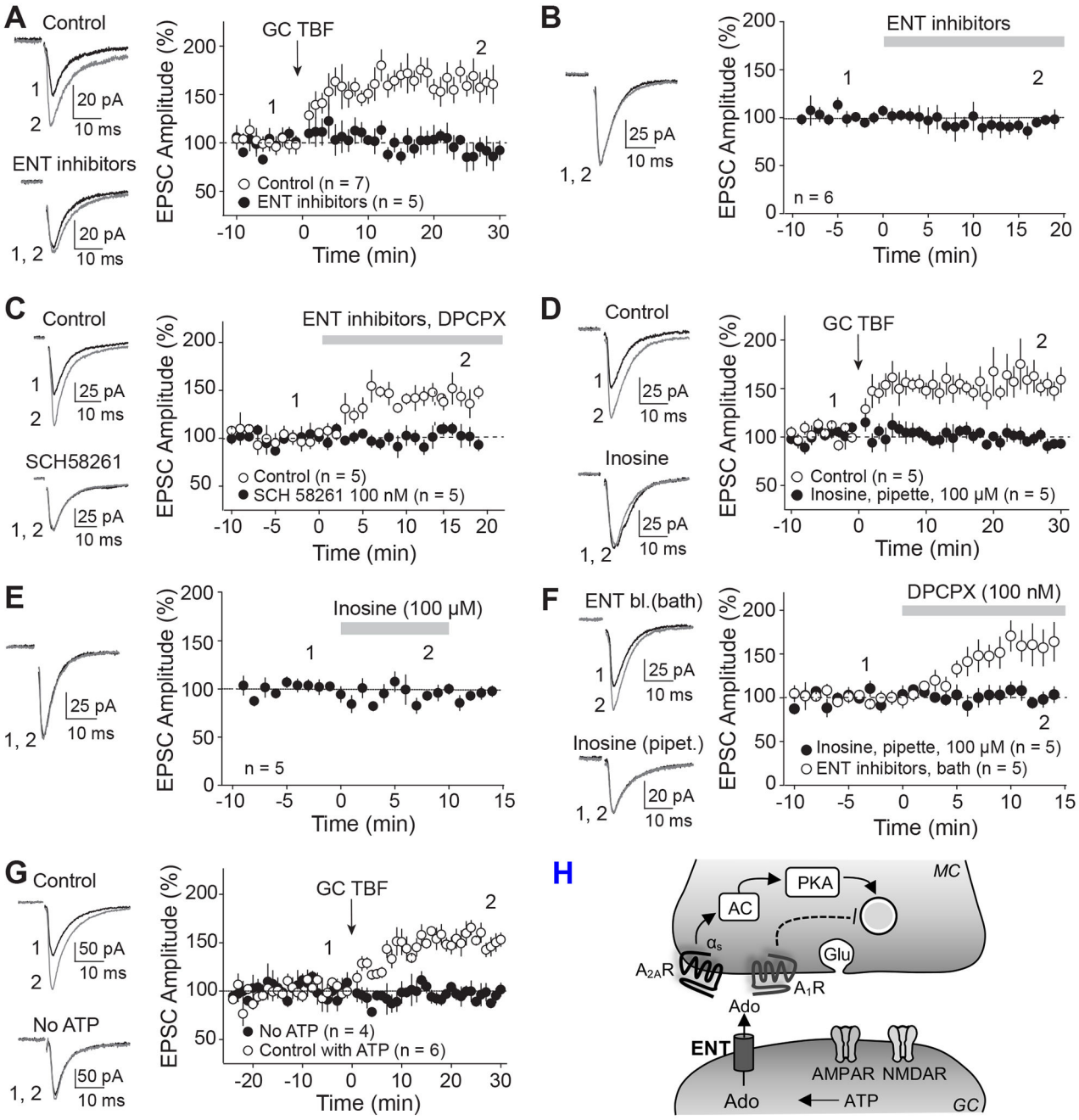

Figure 5: MC-GC LTP requires passive release of adenosine from GCs, via ENTs.

(A) Representative traces *(left)* and time-course summary plot *(right)* showing that GC TBF failed to induce LTP in presence of the ENT blockers (20 μM of dipyridamole and 10 μM of NBMPR) as compared with interleaved controls.

(B) Bath application of the ENT blockers (20 μM of dipyridamole and 10 μM of NBMPR) did not change basal MC-GC EPSC amplitude.

(C) Co-application of the ENT blockers (20 μM of dipyridamole and 10 μM of NBMPR) and the A_1R antagonist DPCPX (100 nM) increased EPSC amplitude in the control condition but not in presence of the $A_{2A}R$ antagonist SCH 58261 (100 nM).
(D) Intracellular loading of inosine (100 μM) via the patch pipette abolished GC TBF-induced LTP.
(E) Time course summary plot (right) and representative traces (left) showing that bath application of inosine (100 μM) did not affect basal EPSC amplitude.
(F) Bath application of DPCPX (100 nM) increased EPSC amplitude when the ENT blockers (20 μM of dipyridamole and 10 μM of NBMPR) were included in the bath but not when inosine (100 μM) was loaded in the postsynaptic neuron via the patch pipette.
(G) GC TBF failed to induce LTP when ATP was removed from the recording solution as compared to controls. To allow for complete intracellular dialysis, LTP induction protocol was applied 25-35 min after break-in.
(H) Scheme summarizing the findings. Adenosine is passively released from GCs via ENTs. Adenosine then activates presynaptic A_1Rs and $A_{2A}Rs$. $A_{2A}R$ activation induces a long-lasting PKA-dependent increase in glutamate (Glu) release, whereas A_1R activation dampens synaptic transmission and LTP.
Numbers in parentheses represent number of cells. Data are represented as mean ± SEM.

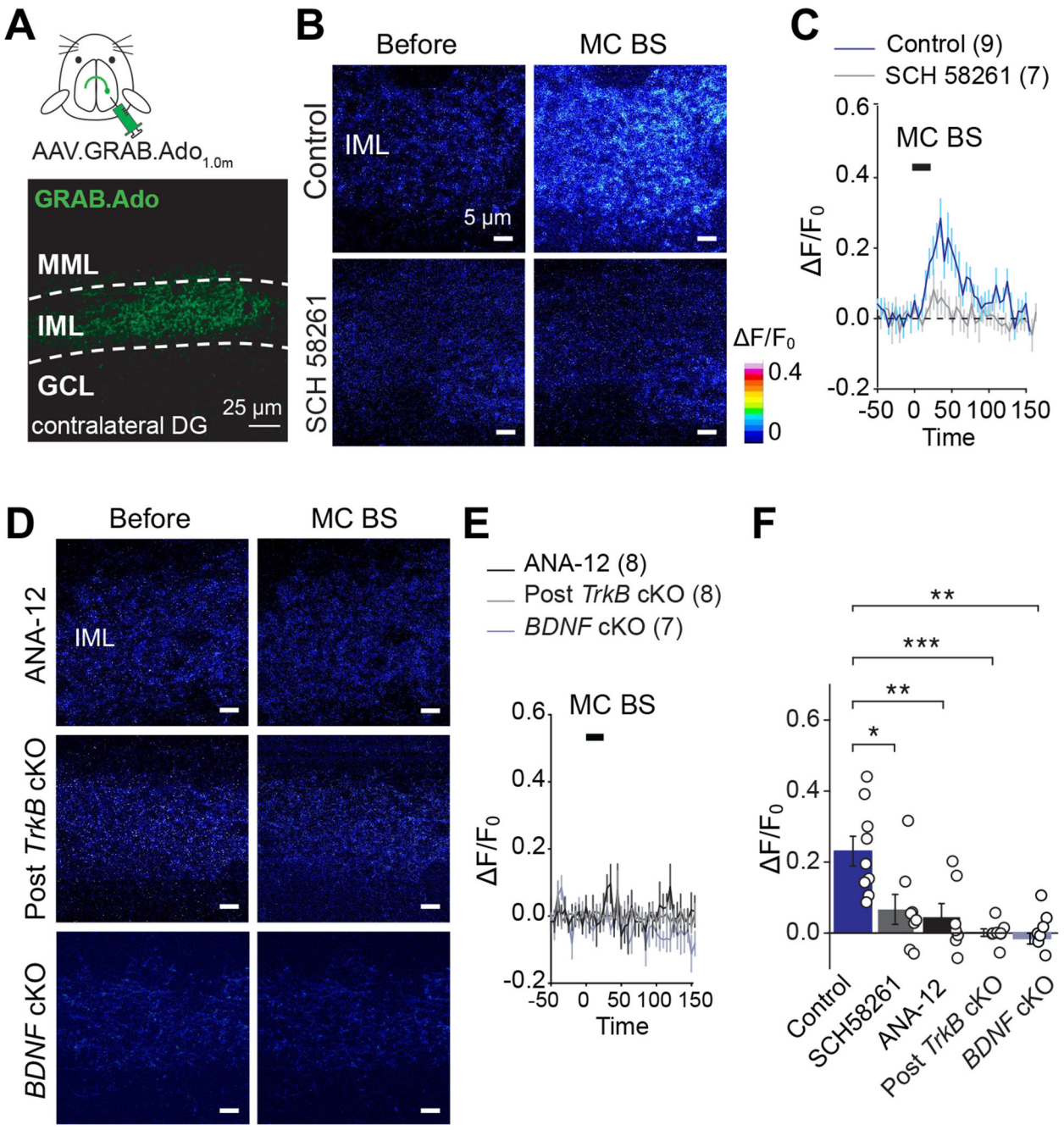

Figure 6: Induction of MC-GC LTP triggers a transient TrkB-dependent increase in extracellular adenosine level

(A) AAV_9.hSyn.GRAB.Ado1.0m ($GRAB_{Ado}$) was injected unilaterally in the DG of WT mice (*top*). Two-photon image (*bottom*) showing $GRAB_{Ado}$ was selectively expressed in putative MC axons in contralateral IML.

(B, C) Two-photon images of the IML **(B)** showing $GRAB_{Ado}$ fluorescence intensity increased during burst electrical stimulation of MC axon terminals (MC BS) in normal ACSF (control) but not in continuous presence of the A_{2A} receptor antagonist SCH 58261

(100 nM). Time-course summary plot of the average fractional fluorescence changes ($\Delta F/F_0$) with time are shown in **C**.

(D, E) Two-photon images of the IML **(D)** and time-course summary plot **(E)** showing how MC BS failed to increase $GRAB_{Ado}$ fluorescence intensity in the continuous presence of the TrkB antagonist ANA-12 (15 μM) and when TrkB (Post *TrkB* cKO) or BDNF (Post *Bdnf* cKO) was conditionally knocked out from GCs.

(F) Quantification of the averaged responses during burst stimulation of MCs (15-25 s) * $p < 0.05$, ** $p < 0.01$, *** $p < 0.001$; one-way ANOVA.

Number of slices are shown between parentheses. Data are represented as mean ± SEM.

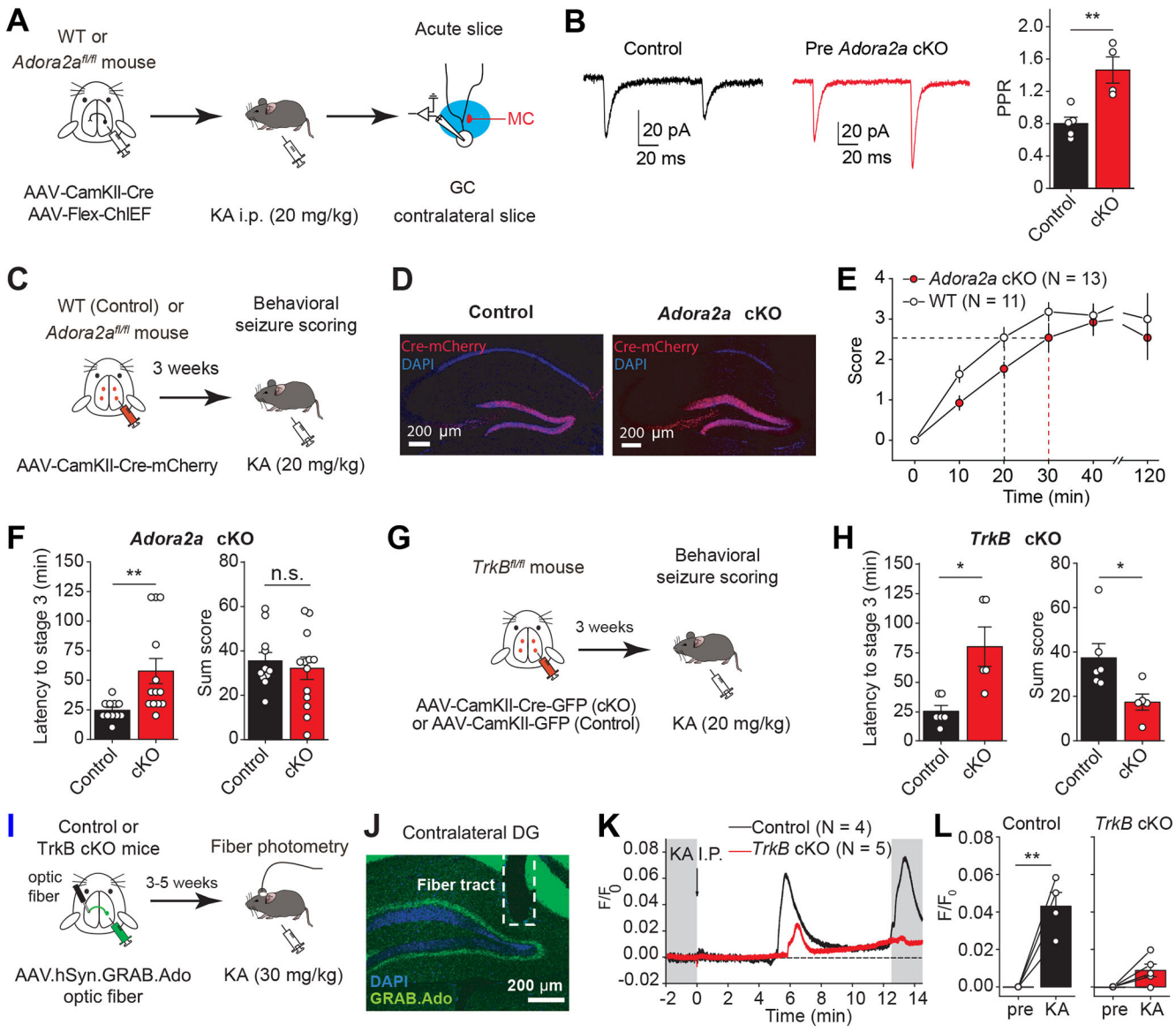

Figure 7: *In vivo* release of adenosine during acute seizures plays a pro-convulsant role by activating A_{2A}Rs

(A) Experimental timeline. A mix of AAV_5.CamKII.Cre-mCherry and AAV_{DJ}.hSyn.Flex.ChIEF.TdTomato was injected unilaterally into the DG of *Adora2a*$^{fl/fl}$ (*Adora2a* cKO) or WT (control) mice. Seizures were induced using a single KA i.p. (20 mg/kg) injection and acute hippocampal slices were prepared 25 min after KA injection. Whole-cell recordings were performed from GC in the contralateral DG and MC-GC light-evoked synaptic responses were monitored.

(B) KA-induced seizures decreased PPR in control but not in presynaptic *Adora2a* cKO conditions. ** $p < 0.01$.

(C) AAV_5-CaMKII-Cre-mCherry was injected bilaterally into ventral and dorsal DG of WT (control) and *Adora2a*$^{fl/fl}$ (cKO) mice. Mouse behavior was assessed for 120 min following KA (20 mg/kg i.p.) administration.

(D) Confocal images showing the viral expression in the DG of WT (control) and *Adora2a*$^{fl/fl}$ (*Adora2a* cKO) mice.
(E, F) Deletion of *Adora2a* from DG excitatory neurons (*Adora2a*$^{f/fl}$ mice injected with AAV_5-CaMKII-Cre-mCherry) significantly increased latency to convulsive seizures **(E, F),** but did not affect seizure severity as compared to control animals. Note the shift in seizure score time course toward the right **(E)**. ** $p < 0.01$, n.s. $p > 0.05$.
(G, H) AAV-CaMKII-eGFP (control) or AAV-CaMKII-Cre-GFP (cKO) was injected bilaterally into ventral and dorsal DG of *TrkB*$^{fl/fl}$ mice. Behavioral seizures were monitored and scored for 120 min **(G)**. Deletion of *TrkB* from hippocampal excitatory neurons induced significant increase in latency to convulsive seizures **(E)** and a decrease in sum score **(H)** and as compared with controls. * $p < 0.05$.
(I) Experimental timeline. AAV_9.hSyn.GRAB.Ado1.0m ($GRAB_{Ado}$) was injected unilaterally in the DG of *TrkB*$^{fl/fl}$ mice. In the contralateral DG, both control (AAV-CaMKII-mCherry) or Cre-expressing AAV (AAV-CaMKII-Cre-mCherry, TrkB cKO) was injected and an optic fiber was implanted above the contralateral IML. Fiber photometry was performed 3-5 weeks later to assess $GRAB_{Ado}$ fluorescence intensity before and after acute seizure induction with kainic acid (KA, 30 mg/kg i.p.), in control and *TrkB* cKO mice.
(J) Confocal image showing fiber tract and $GRAB_{Ado}$ expression in the contralateral IML.
(K, L) Time-course of a control and a *TrkB* cKO representative experiments **(K)** and summary histogram **(L)** showing how KA (30 mg/kg i.p.) administration increased the average fractional fluorescence ($\Delta F/F_0$) of $GRAB_{Ado}$ in control mice, an effect that was significantly reduced in *TrkB* cKO animals. ** $p < 0.01$, n.s. $p > 0.05$.
Numbers in parentheses represent number of mice. Data are presented as mean ± SEM.

KEY RESOURCES TABLE

REAGENT or RESOURCE	SOURCE	IDENTIFIER
Antibodies		
guinea pig anti-$A_{2A}R$ polyclonal	Frontier Institute co	AB_2571656
rabbit anti-A_1R	Affinity Bioreagents, Labome	AAR-006
goat anti-guinea pig IgG coupled to 1.4 nm gold	Nanoprobes Inc.	Cat# 2054
goat anti-rabbit IgG coupled to 1.4 nm gold	Nanoprobes Inc.	Cat# 2003
Bacterial and virus strains		
AAV5-CamKII-GFP-Cre	Penn Vector Core	AV-5-PV2521
AAV5-CamKII-eGFP	Penn Vector Core	AV-5-PV1917
AAV5-CamKII-Cre-mCherry	UNC Vector	N/A
AAV5-CamKII-mCherry	UNC Vector, plasmid deposited by Dr. Karl Deisseroth, Stanford University	N/A
AAVDJ.Flex.ChIEF.Tdtomato	Dr. Pascal Kaeser	N/A
LV-CIQL2-ChiEFtom2A-Cre (ChIEFtom2A-Cre)	Drs. Gaël Barthet and Christopher Mulle, Université de Bordeaux	N/A
LV-CIQL2-ChiEFtom2A-GFP (ChiEFtom2A-GFP)	Drs. Gaël Barthet and Christopher Mulle, Université de Bordeaux	N/A
AAV9.hSyn.GRAB.Ado1.0m	WZ Biosciences Inc	YL005006-AV9
Chemicals, peptides, and recombinant proteins		
Picrotoxin	Sigma-Aldrich	Cat#P1675
CGP55845 hydrochloride	HelloBio	HB0960
PKI_{14-22} amide, myristoylated	Tocris Bioscience	Cat#2546
PKI_{6-22} amide	Tocris Bioscience	Cat#1904
DCG-IV	Tocris Bioscience	Cat#0975
ANA-12	Tocris Bioscience	Cat#4781
Botulinum toxin-B	List biological	Cat# 620A
H89 dihydrochloride	Tocris Bioscience	Cat#2910
D-APV	HelloBio	HB0225
NBQX disodium salt	HelloBio	HB0443
Kainic acid	HelloBio	HB0355
L-NAME	Tocris Bioscience	Cat#0665
Baicalein	Tocris Bioscience	Cat#1761
AACOCF3	Tocris Bioscience	Cat#1462
THL (orlistat)	Tocris Bioscience	Cat#3540
SCH 58261	Tocris Bioscience	Cat#2270
ZM 241385	Tocris Bioscience	Cat#1036
BDNF (human)	Tocris Bioscience	Cat#2837
$GDP_{\beta s}$	Sigma-Aldrich	Cat# G7637
Baclofen	Tocris Bioscience	Cat#0796

REAGENT or RESOURCE	SOURCE	IDENTIFIER
DPCPX	Tocris Bioscience	Cat#0439
CGS 21680 hydrochloride	Tocris Bioscience	Cat#1063
Inosine	Sigma-Aldrich	Cat# I4125
dipyridamole	Tocris Bioscience	Cat#0691
NBMPR	Tocris Bioscience	Cat# 2924
CCPA	Tocris Bioscience	Cat# 1705
Experimental models: Organisms/strains		
Rat: Sprague-Dawley	Charles River	Cat# 400
Mouse: C57BL/6NCrl	Charles River	Cat# 027
Mouse: *TrkB*$^{fl/fl}$	Dr. Lisa Monteggia	N/A
Mouse: BDNF$^{fl/fl}$	Dr. Lisa Monteggia	N/A
Mouse: A2A$^{fl/fl}$: B6;129-Adora2atm1Dyj/J,	Jax Lab	Cat# 010687
Mouse: VGluT2-Cre: Slc17a6$^{tm2(cre)Lowl}$/J	Jax Lab	Cat# 016963
Software and algorithms		
IgorPro	Wavemetrics	https://www.wavemetrics.com/
OriginPro 9	OriginLab	http://www.originlab.com/